

Group, field and isolated early-type galaxies

I. Observations and nuclear data

G. Denicoló,^{1*} Roberto Terlevich,^{2†} Elena Terlevich,^{2†} Duncan A. Forbes,³ Alejandro Terlevich,⁴ Luis Carrasco²

¹*Institute of Astronomy, Madingley Road, Cambridge, CB3 0HA, United Kingdom*

²*Instituto Nacional de Astrofísica, Óptica y Electrónica, Tonantzintla, Puebla, Mexico*

³*Centre for Astrophysics & Supercomputing, Swinburne University, Hawthorn, VIC 3122, Australia*

⁴*School of Physics and Astronomy, University of Birmingham, Edgbaston, Birmingham, B15 2TT, United Kingdom*

Accepted. NOvember 3rd 2004 Received; in original form 2004 July

ABSTRACT

This is the first paper of a series on the investigation of stellar population properties and galaxy evolution of an observationally homogeneous sample of early-type galaxies in groups, field and isolated galaxies.

Here we present high signal-to-noise long-slit spectroscopy of 86 nearby elliptical and S0 galaxies. Eight of them are isolated, selected according to a rigorous criterion, which guarantees a genuine low-density sub-sample. The present survey has the advantage of covering a larger wavelength range than normally found in the literature, which includes [O III] $\lambda 5007$ and H α , both lines important for emission correction. Among the 86 galaxies with $S/N \geq 15$ (per resolution element, for $r_e/8$ central aperture), 57 have their H β -index corrected for emission, the average correction is 0.190 Å in H β ; 42 galaxies reveal [O III] $\lambda 5007$ emission, of which 16 also show obvious H α emission. Most of the galaxies in the sample do not show obvious signs of disturbances nor tidal features in the morphologies, although 11 belong to the Arp catalogue of peculiar galaxies; only three of them (NGC 750, NGC 751, NGC 3226) seem to be strongly interacting. We present the measurement of 25 *central* line-strength indices calibrated to the Lick/IDS system. Kinematic information is obtained for the sample. We analyse the line-strength index *vs* velocity dispersion relations for our sample of mainly low density environment galaxies, and compare the slope of the relations with cluster galaxies from the literature. Our main findings are that the index- σ_0 relations presented for low-density regions are not significantly different from those of cluster E/S0s. The slope of the index- σ_0 relations does not seem to change for early-type galaxies of different environmental densities, but the scatter of the relations seems larger for group, field and isolated galaxies than for cluster galaxies.

Key words: galaxies: stellar content – galaxies: abundances – galaxies: elliptical and lenticular – galaxies: nuclei – galaxies: kinematics and dynamics

1 INTRODUCTION

The standard paradigm for galaxy formation is one of hierarchical clustering and subsequent merging to form progressively larger galaxies (White & Rees 1978). All galaxies are located within dark matter halos, and the properties of galaxies depend on the assembly history of these dark mat-

ter halos and hence their environment. This process has been modelled by semi-analytical methods (e.g. Baugh *et al.* 1998; Kauffmann *et al.* 1999; Somerville & Primack 1999) and by hydrodynamical simulations (e.g Cen & Ostriker 1992; Pearce *et al.* 1999; Berlind *et al.* 2003). For example, Kauffmann & Charlot (1998) predict that galaxies in low density environments are younger (in a luminosity weighted sense) on average than those in clusters as they have a more extended merger history. They also predict that massive ellipticals are younger than smaller ones, again due to merger-induced star formation. Quantitative predictions depend on

* Visitor at INAOE, Mexico.

† Visiting Fellow, IoA, Cambridge. E-mail for contact:
rjt@inaoep.mx and *eterlevi@inaoep.mx*

the details of the gas physics and feedback processes (e.g. Kay *et al.* 2002; Kauffmann *et al.* 2004). High quality data already exists for the cluster ellipticals, thus *determining the ages and metallicities of field and group ellipticals is a key test of the HCM paradigm* (González 1993; Bower *et al.* 1998; Trager *et al.* 2000a,b; Kuntschner 2000; Terlevich & Forbes 2002; Chiosi & Carraro 2002; Kuntschner *et al.* 2002; Willis *et al.* 2002).

In an effort to disentangle the degeneracy of age and metallicity effects on the gross properties of stellar populations, Worthey (1994, 1997) developed a series of stellar population spectral synthesis models. He showed that certain predominantly age (i.e. H β , H γ) and metallicity (i.e. Fe, [MgFe]) sensitive spectral absorption features can break the degeneracy, and the luminosity weighted mean ages and metallicities can be determined. In a study of bright galaxies in the Fornax cluster, Kuntschner & Davies (1998) showed that, as predicted by the high z studies, the cluster ellipticals are indeed uniformly old, and span a range in metallicities. However, earlier studies of field (and loose group) ellipticals (González 1993; Trager 1997) seem to show just the opposite, displaying a uniform metallicity, but spanning a range in ages. This suggests the possibility of an *environmental dependence* of the colour-magnitude relation (CMR), or maybe two completely different mechanisms operating in cluster and field environments, conspiring to produce similar CMRs. *The universality of the CMR from cluster core to the field environments, and its interpretation as a metallicity sequence, is fundamental to its placing a limit on the formation epoch of cluster elliptical galaxies to $z > 1$* (e.g. Bower, Lucey & Ellis 1992). If there is in fact a conspiracy between age and metallicity producing a tight CMR, this limit could be significantly loosened.

We have carried out a large and observationally homogeneous survey of local early-type galaxies in low density environments with the aim of determining nuclear parameters, kinematic, age and metallicity gradients. This will help to infer whether the central values represent a small localised starburst or whether the whole galaxy was involved. The spectra, when combined with existing photometry, will allow us to investigate scaling relations such as the fundamental plane, Mg- σ and colour-magnitude relations for field galaxies, and directly compare how these relations agree with galaxy formation histories, from their mean ages and metallicities. The luminosity weighted mean ages and metallicities of these galaxies will also allow us to directly test fundamental predictions of hierarchical models for structure formation in the universe. The emission line data will allow the discrimination among the different ionization mechanisms and provide information about the kinematical status of the ionized gas. In this paper we present the data, central measures and comparisons with previous work.

The paper is divided as follows. In Section 2 we describe the sample selection, and Section 3 details the observations and data reduction procedures. Section 4 describes the transformation of spectral index measurements to the Lick/IDS system, an improved method for emission correction of the Balmer line indices, and the derivation of errors from repeated measurements. We explain the determination of kinematical properties and errors in Section 5. Section 6 presents the finally corrected line-strength indices. In Section 7 we analyse the index *vs* central velocity dispersion

relations. Our results are summarized in Section 8. Complementary information about the sample and fully corrected Lick indices are presented in Appendices A and B.

2 SELECTION OF GALAXIES

We have selected early-type galaxies that lie in relatively low density environments, i.e., in loose groups (56), the general field (19) and truly isolated galaxies (8). However, we also observed 3 Virgo cluster galaxies, to complete a total of 86 galaxies. The objects are distributed all over the sky but with strong concentrations around the galactic poles and away from the galactic plane. Galaxies in groups come from the group catalogue of Garcia (1993).

Eight galaxies were classified as truly isolated by Reda *et al.* (2004). Below, we describe briefly how isolated galaxies were selected. By using the *Lyon-Meudon Extragalactic Data Archive* (LEDA) of $\sim 100,000$ galaxies, the following criteria were applied:

- Morphological type $T \leq -3$
- Virgo corrected recession velocity $V \leq 9000 \text{ km s}^{-1}$,
- Apparent Magnitude $B_T \leq 14.0$.

This produced 330 galaxies which could be considered as potential isolated galaxies. The galaxies were compared to the rest of the catalogue and accepted as being isolated if they had no neighbours which were:

- within 700 km s^{-1} in recession velocity,
- within 0.67 Mpc in the plane of the sky (assuming $H_0 = 75 \text{ km s}^{-1} \text{ Mpc}^{-1}$),
- less than 2 magnitudes fainter in B_T .

Lastly, in the process of determining isolated objects, all galaxies were checked visually on the *Digitised Sky Survey* (DSS) images to ensure no near projected galaxy. This produced a final list of 40 early-type isolated galaxies; in this work we have obtained spectra of 8 of them.

By exclusion, non-cluster galaxies which are not associated with groups and also not identified as isolated galaxies are then assumed to lie in the general field.

The Tully (1987) local density parameter ρ is available for about 3/4 of our sample. Values range from 0.08 (isolated) to 3.99 (a Virgo galaxy). The sample also shows a good overlap with the Lick/IDS system, with 59 galaxies in common (Trager *et al.* 1998).

3 OBSERVATIONS AND DATA REDUCTION

Long-slit spectra have been obtained, during five different runs, accounting for a total of 30 nights, at the 2.12 m telescope of *Observatorio Astrofísico Guillermo Haro* (OAGH), in Cananea, Mexico. The telescope is equipped with a Boller & Chivens spectrograph and a Tek 1024 pix² CCD camera. Parameters of the observations are reported in Table 1. We have obtained spectra in two wavelength ranges (blue and red), covering a total range from $\sim 3850 \text{ \AA}$ to $\sim 6700 \text{ \AA}$. Two 300 lines mm⁻¹ grating blazed at 4650 \AA and 5900 \AA (for the blue and red wavelength ranges, respectively) yielded a dispersion of 65 \AA mm^{-1} on the spectrograph CCD, i.e.,

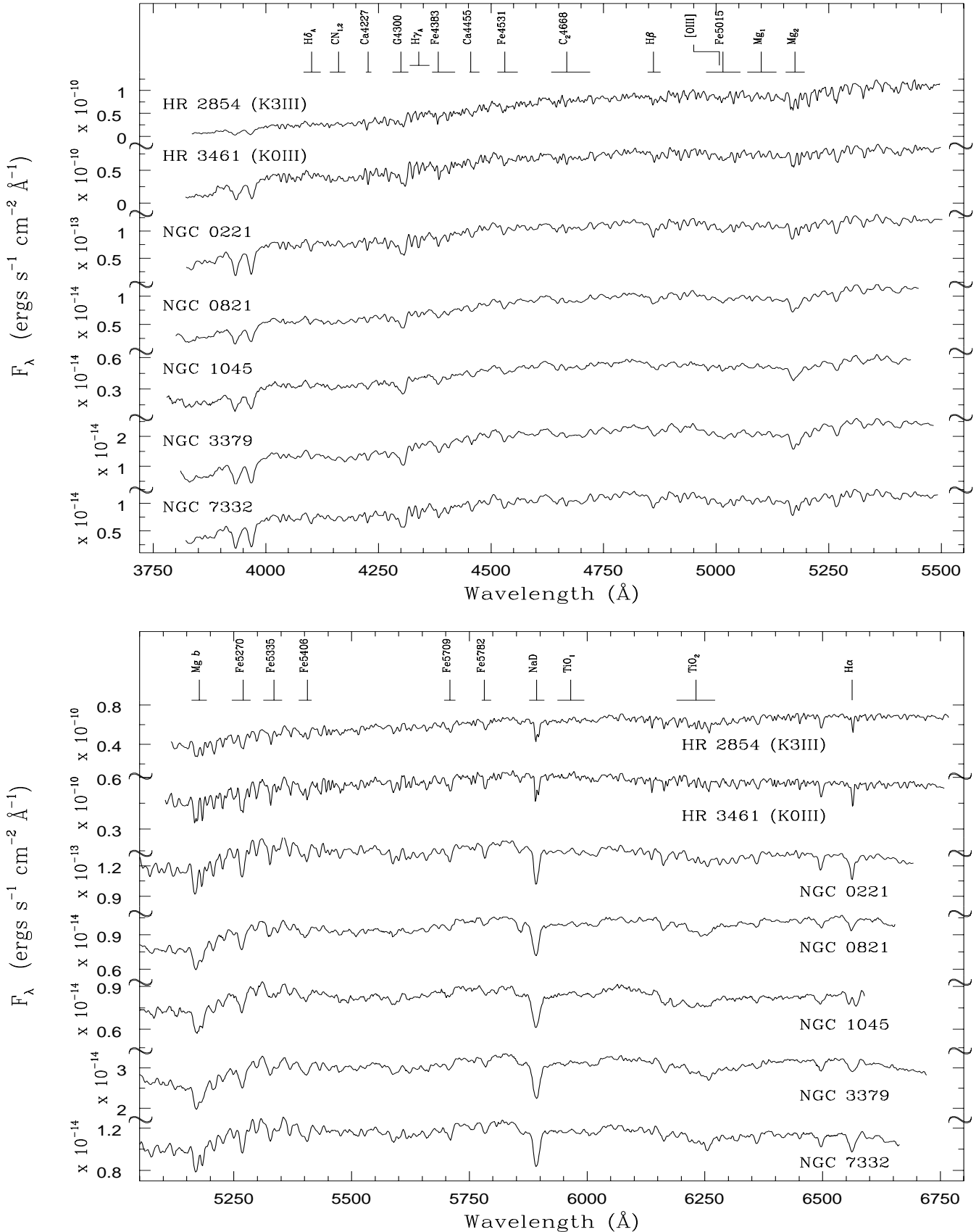


Figure 1. Typical spectra of two stars and five galaxies. The top panel shows the spectra in the blue wavelength range, the bottom panel presents the red wavelength range. All spectra are flux calibrated using standard Oke (1990) stars. The galaxy spectra are redshift corrected and represent the nuclear $r_e/8$ extraction.

an instrumental dispersion of $\sim 1.6 \text{ \AA}/\text{pixel}$. Typically, exposure times were between 300 to 1200 seconds per galaxy frame. Total exposure times were chosen to obtain $S/N > 40$ per \AA at 5000\AA . The slit has been centred on the nucleus and oriented along the major axis for most of the galaxies. We observed the galaxies close to minimum zenithal distance in order to minimize differential refraction effects. Some neighbouring galaxies have been observed along the line connecting their nuclei. Instrumental resolution of $\sim 6 \text{ \AA}$ (FWHM) was achieved with a slit width of 1.5 arcsec. Table 2 presents the detailed listing of the galaxy observations. The seeing was generally better than 2.0 arcsec. Additionally we observed 46 different standard stars (mainly K-giants) to be used as templates for velocity dispersion measurements, and for calibration of the line-strength indices to the Lick/IDS system (González 1993). Six spectrophotometric standard stars were also taken to enable flux calibration. At least two different spectrophotometric standard stars were observed per night. Table 3 lists all observed stars with their spectral types (obtained from SIMBAD, operated by CDS, Strasbourg). In addition, a bona fide elliptical galaxy, NGC 3379, was observed in every run to serve as a link galaxy for the measurement of indices and velocity dispersion between the different observing runs.

All data reduction was performed using packages in **IRAF**. Each frame has been treated separately. Initial reduction of the CCD frames involved overscan correction, bias subtraction, the removal of pixel-to-pixel sensitivity variations (using dome flat exposures), and correction for uneven illumination along the slit (using twilight sky exposures). Careful wavelength calibration was performed using He-Ar or Fe-Ar lamp exposures. For the blue wavelength range observations ($\sim 3850\text{-}5450 [\text{\AA}]$), He-Ar lamps were taken before and after each exposure to achieve an accurate wavelength calibration. For the red wavelength range ($\sim 5100\text{-}6700 [\text{\AA}]$), we followed the same procedure using Fe-Ar lamps. A linear fit between pixel number and wavelength for ~ 30 arc lines gave an rms calibration error $<0.1 \text{ \AA}$ in most cases. The galaxy frames were then corrected for atmospheric extinction, and afterwards, the continuum shape of the spectra was corrected to a relative flux scale with the help of the spectrophotometric standard stars. The cosmic rays were cleaned with the task **crmedian**, which detects cosmic rays from pixels deviating by a 3-sigma level from the median at each pixel. Sky subtraction was then performed in each frame and finally, we used the task **apall** to extract 1d-spectra. We have extracted the central $r_e/8$ (r_e is the effective radius[†]) from all galaxy frames, and these extractions will be used as our standard nuclear observations. A sample of seven typical spectra is shown in Figure 1.

The signal-to-noise ratio (S/N) per resolution element (resolution element = 6 \AA FWHM) of individual 1-D galaxy extractions ranges from 9 to about 100. The signal-to-noise was estimated assuming Poisson statistics, \sqrt{N} , where N is the number of photon counts. The gain of the CCD, as presented in Table 1, is $1.85 \text{ e}^-/\text{ADU}$, and therefore the mean number of counts in the spectra was multiplied by the gain to obtain the photon statistics. The S/N measurement was performed in regions of $\sim 120 \text{ \AA}$ encompassing the continua

[†] Effective radii are from Trager *et al.* 2000b and RC3.

Table 1. Instrumental set-up.

Telescope	OAGH 2.12 m, Cananea, Mexico	
	Blue	Red
Spectral range [\AA]	3850-5450	5100-6700
Date of observations	2000 Mar 25-29 2000 Apr 01-02 2000 Oct 20-26 2001 Oct 13,18-19 2002 Apr 08	2000 Mar 30-31 2000 Apr 03 2001 Mar 27-29 2001 Oct 14-17 2002 Apr 06-07
Spectrograph	B & C	B & C
Detector	CCD Tek 1024	CCD Tek 1024
Gain [e^-/ADU]	1.85	1.85
Read-out-noise [$e^- \text{ rms}$]	3.7	3.7
Pixel size [μm^2]	24	24
Spatial scale ["/pixel]	0.44	0.44
Slit length [']	3	3
Slit width ['']	1.5	1.5
Grating [lines/mm]	300	300
Dispersion [$\text{\AA}/\text{pixel}$]	~ 1.6	~ 1.6
Resolution [\AA]	~ 6	~ 6
Seeing [arcsec]	1.5-2	1.5-2

of Mg_2 index or the continua of TiO_2 index, for the blue or red spectra, respectively.

We have only performed equivalent width measurements in spectra with $S/N \geq 15$ per resolution element. We opted to work with the galaxy frames separately to avoid any possible wavelength mismatch when combining the frames. This decision offers statistical advantages as we are working with ~ 700 spectral frames of $S/N \geq 15$ (per resolution element) for a sample consisting of a total of 86 different galaxies (total of 8 frames/galaxy on average, where 4 frames are in the red wavelength range and 4 frames in the blue spectral range, in general). The line-strength index measurements were therefore performed in all spectra separately and later averaged for each galaxy.

The median S/N per frame is ~ 40 per resolution element (Figure 2). The effective S/N per galaxy can then be estimated as, approximately, the square-root of the number of frames per galaxy times the median S/N per frame, i.e., effective S/N per galaxy in the blue *or* red spectral range (average of 4 frames per galaxy *per spectral range*) $\approx \sqrt{4} \times 40 \simeq 80$ per resolution element.

Finally, we refer to the data in this paper as the OAGH sample.

4 LICK INDICES

Absorption line indices in the visual as defined by the Lick group (e.g., $\text{H}\beta$, Mg_2 , $\text{Fe}5270$, $\text{Fe}5335$, etc, Burstein *et al.* 1984; Faber *et al.* 1985) have proven to be a useful tool for the derivation of ages and metallicities of unresolved stellar populations.

Our spectra cover the 21 Lick indices defined in Faber *et al.* (1985) and Worthey *et al.* (1994), and the subsequent four Balmer indices ($\text{H}\delta_{A,F}$, $\text{H}\gamma_{A,F}$) first presented in Worthey & Ottaviani (1997). The indices are calculated by the standard equations:

Table 2. Log of observations: galaxies.

Galaxy	Classification	B_T [mag]	Exp. Blue	Exp. Red	PA [°]	Galaxy	Classification	B_T [mag]	Exp. Blue	Exp. Red	PA [°]
ESO 462-G015	E3	12.95	3600	6300	166	NGC 3599	SA0	12.82	9600	3600	20
MCG -01-02-018	(R')SA(r)0	14.23	3600	3600	170	NGC 3607	SA0	10.82	2700	2700	120
NGC 0016	SAB0	13.00	3600	2700	20	NGC 3608	E2	11.70	3600	2700	75
NGC 0221	cE2	9.03	3600	2700	90	NGC 3610	E5	11.70	3600	3600	130
NGC 0315	E+ LINER-Sy1	12.20	5400	2700	55	NGC 3613	E6	11.82	3600	1800	102
NGC 0474	SA(s)0	12.37	4800	2700	90	NGC 3636	E0	12.82	4800	2400	90
NGC 0584	E4	11.44	3600	2700	55	NGC 3640	E3	11.36	3600	2400	100
NGC 0720	E5	11.16	2700	2700	140	NGC 3665	SA(s)0	11.77	3600	1800	130
NGC 0750	E pec	12.89	4800	3600	166	NGC 3923	E4-5	10.80	1200	2700	45
NGC 0751	E pec	13.50	4800	3600	166				1200		90
NGC 0777	E1	12.49	3600	4800	155	NGC 3941	SB(s)0 Sy2	11.25	3600	1800	90
NGC 0821	E6	11.67	2700	2700	32	NGC 4125	E6 pec LINER	10.65	4800	1800	80
NGC 0890	SAB(r)0	12.20	3600	2700	140	NGC 4261	E2-3 LINER	11.41	3600	900	90
NGC 1045	SA0 pec	13.52	3600	2700	40	NGC 4365	E3	10.52	3600	2700	40
NGC 1052	E4 LINER-Sy2	12.08	2700	2700	122	NGC 4374	E1 LINER	10.09	1800	900	90
NGC 1132	E	13.25	3600	6300	140	NGC 4494	E1-2	10.71	3600	1800	180
NGC 1407	E0	10.70	2700	1800	180	NGC 4550	SB0	12.56	3600	1800	90
NGC 1453	E2-3	12.77	3600	2700	45			1200			35
NGC 1600	E3	11.93	3600	2700	15	NGC 4754	SB(r)0	11.52	3600	1800	115
NGC 1700	E4	12.20	2400	6300	90	NGC 5322	E3-4 LINER	11.14	4800	3600	95
NGC 1726	SA(s)0	12.66	4500	5100	180	NGC 5353	S0	11.96	4800	4800	180
NGC 2128	S0	13.60	8400	7200	140	NGC 5354	SA0 LINER	12.33	4800	3600	90
NGC 2300	SA0	12.07	9900	9900	180	NGC 5363	I0 LINER	11.05	5400	2700	135
NGC 2418	E	13.16	7500	6600	50	NGC 5444	E+	12.78	4800	2400	67
			2700		35	NGC 5557	E1	11.92	3600	1800	90
NGC 2513	E	12.59	8400	3600	90	NGC 5576	E3	11.85	3600	1800	90
NGC 2549	SA(r)	12.19	3600	1800	90	NGC 5638	E1	12.14	3600	1800	170
NGC 2768	S0 LINER	10.84	3600	1800		NGC 5812	E0	12.19	4800	2400	90
			2700		90	NGC 5813	E1-2	11.45	7200	5400	145
NGC 2872	E2	12.86	4800	2400	110	NGC 5831	E3	12.45	6000	2400	90
NGC 2911	SA0 pec Sy	12.50	6000	9300	50	NGC 5845	E:	13.50	8400	2400	120
NGC 2974	E4	12.30	3600	2400	135	NGC 5846	E0-1 LINER-HII	11.05	7200	4500	180
NGC 3091	E3	12.13	2700	1800	90			1800			90
NGC 3098	S0	12.89	6000	3600	180	NGC 5846A	cE2-3	14.10	7200	4500	180
NGC 3115	S0	9.87	2700	2280	135	NGC 5854	SB(s)0	12.71	4800	3600	155
NGC 3139	S0 pec	15.00	2700	1800	90	NGC 5864	SB(s)0	12.77	3600	2400	155
NGC 3156	S0	13.07	4800	2700	40	NGC 5869	S0:	12.91	2700	1800	120
NGC 3193	E2	11.83	3600	2700	90	NGC 5982	E3	12.04	3600	1800	114
NGC 3226	E2 pec LINER	12.30	4800	2400	90	NGC 6172	E+	13.83	8400	9900	80
NGC 3245	SA(r)0 HII-LINER	11.70	3600	1800	90	NGC 6411	E	12.79	2700	7200	60
NGC 3377	E5-6	11.24	3600	1800	135	NGC 7302	SA(s)0	13.58	4800	6300	100
NGC 3379	E1 LINER	10.24	8100	3600	90	NGC 7332	S0 pec	12.02	6300	5400	155
			3600	1800	70	NGC 7454	E4	12.78	3600	2700	148
NGC 3384	SB0	10.85	2700	1800	53	NGC 7585	(R')SA(s)0 pec	12.50	3600	2700	115
NGC 3412	SB(s)0	11.45	3600	1800	45	NGC 7619	E	12.10	7200	5400	30
NGC 3414	S0 pec	11.96	4800	3600	110	NGC 7626	E pec	12.16	7200	5400	90
			2700		25						

Classification and apparent magnitude (B_T) information from NED (2003).

$$EW_A^\circ = \int_{\lambda_1}^{\lambda_2} \left(1 - \frac{F(\lambda)}{C(\lambda)} \right) d\lambda, \quad (1)$$

$$EW_{mag} = -2.5 \log \left(\frac{\int_{\lambda_1}^{\lambda_2} \frac{F(\lambda)}{C(\lambda)} d\lambda}{\lambda_2 - \lambda_1} \right), \quad (2)$$

where

$$C(\lambda) = F_b \frac{\lambda_r - \lambda}{\lambda_r - \lambda_b} + F_r \frac{\lambda - \lambda_b}{\lambda_r - \lambda_b}, \quad (3)$$

λ_b and λ_r are the mean wavelength in the blue and red pseudocontinuum intervals respectively. We have adopted the

spectral pseudocontinua and bandpasses of the 25 Lick/IDS indices defined in Worthey *et al.* (1994) and Worthey & Ottaviani (1997).

The conversion between *suitable equivalent widths* (EW_A°) and magnitude indices is given by

$$Index' = -2.5 \log \left(1 - \frac{Index}{\Delta\lambda} \right) \quad (4)$$

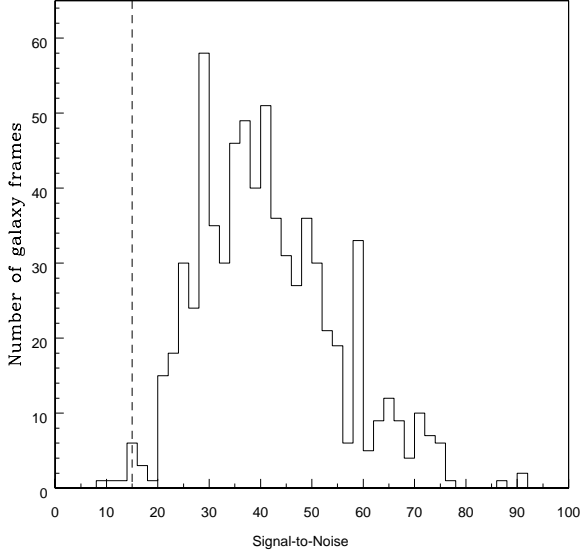
where $\Delta\lambda$ is the width of the index bandpass.

In this work we will use the index combination [MgFe] defined in Thomas, Maraston & Bender (2003, TMB03). Note: in their paper this index is called [MgFe]', but we will

Table 3. Log of observations: stars.

Star	Type	Comment	Star	Type	Comment
HR 0166	K0V	Lick/IDS std	HR 6770	G8III	Lick/IDS std
HR 1015	K3III	Lick/IDS std	HR 6806	K2V variable	Lick/IDS std
HR 1907	K0IIIb	Lick/IDS std	HR 6817	K1III	Lick/IDS std
HR 2429	K1III variable	Lick/IDS std	HR 6872	K2III variable	Lick/IDS std
HR 2459	K5III	Lick/IDS std	HR 7149	K2III	Lick/IDS std
HR 2574	K4III	Lick/IDS std	HR 7176	K1III	Lick/IDS std
HR 2697	K2III variable	Lick/IDS std	HR 7185	B5IV	
HR 2854	K3III	Lick/IDS std	HR 7317	K4III	Lick/IDS std
HR 2970	G9III	Lick/IDS std	HR 7480	A3IV	
HR 3145	K2III	Lick/IDS std	HR 7576	K3III	Lick/IDS std
HR 3461	K0III	Lick/IDS std	HR 7596	A0III	
HR 3845	K2.5III variable	Lick/IDS std	HR 7914	G5V	Lick/IDS std
HR 3905	K2III	Lick/IDS std	HR 7957	K0IV	Lick/IDS std
HR 5370	K3III variable	Lick/IDS std	HR 8165	K1III	Lick/IDS std
HR 5480	G7III variable	Lick/IDS std	HR 8430	F5V	Lick/IDS std
HR 5744	K2III variable	Lick/IDS std	HR 8665	F7V	Lick/IDS std
HR 5854	K2IIIb	Lick/IDS std	HR 8772	F8V	Lick/IDS std
HR 5888	G8III	Lick/IDS std	HR 8832	K3V	Lick/IDS std
HR 5901	K1IVa	Lick/IDS std	HR 8841	K0III	Lick/IDS std
HR 5940	K1IV	Lick/IDS std	HR 8924	K3III variable	Lick/IDS std
HR 6014	K1.5IV	Lick/IDS std	HR 8969	F7V	Lick/IDS std
HR 6018	K1III-IV variable	Lick/IDS std	BD+25 4655	?e...	spec. std (Oke 1990)
HR 6136	K4III	Lick/IDS std	BD+33 2642	B2IVp	spec. std (Oke 1990)
HR 6159	K4III variable	Lick/IDS std	BD+75 325	O5p variable	spec. std (Oke 1990)
HR 6299	K2III variable	Lick/IDS std	Feige 34	DA:	spec. std (Oke 1990)
HR 6458	G0V variable	Lick/IDS std	G 191-B2B	DAw...	spec. std (Oke 1990)
HR 6710	F2IV	Lick/IDS std	Hz 44	B2	spec. std (Oke 1990)

Stellar type information from SIMBAD (2003).

**Figure 2.** Signal-to-noise ratio (per resolution element) for individual frames of our galaxy sample using $r_e/8$ central extractions. Index measurements were only performed in spectra with $S/N \geq 15$ per resolution element (as shown by the dashed line).

adopt simply the notation $[\mathrm{MgFe}]$ for their same definition), and given by equation 5, which should be completely independent of α/Fe variations, according to their models. We also use the index $\langle \mathrm{Fe} \rangle$ as the average given by equation 6 (defined by Kuntschner 1998):

Table 4. Adopted resolutions to match Lick/IDS.

Wavelength [Å]	FWHM [Å]
~3850 - 4200	11.2
4200 - 4650	9.2
4651 - 5150	8.4
5151 - 5700	8.4
5701 - ~6700	9.8

$$[\mathrm{MgFe}] = \sqrt{Mgb \cdot (0.72 \cdot Fe5270 + 0.28 \cdot Fe5335)} \quad (5)$$

$$\langle \mathrm{Fe} \rangle = (Fe4383 + Fe5270 + Fe5335)/3 \quad (6)$$

Before measuring the indices, the galaxy spectra were convolved with gaussian curves in order to degrade their resolution to match the Lick/IDS data resolution. We have adopted the average values in the Lick/IDS resolution curve presented in Worthey & Ottaviani (1997). The values we used are summarized in Table 4. We assume that the Lick/IDS resolution continues to degrade to the blue and red end, where we extrapolated the wavelength limits from Worthey & Ottaviani (1997).

4.1 Index errors

A central aspect of this work is that the determination of the errors in all measured and derived parameters is based on the analysis of the distribution of repeated observations.

We consider that the determination of errors through

multiple observation is more reliable than estimates based on photon statistics of object and sky, detector noise, flat field errors, etc (e.g., Cardiel *et al.* 1998). This is because in the repeated observations all main sources of random error are included by default. Furthermore, no assumption about the error distribution function shape is necessary to determine its moments.

Care was taken in order to observe our sample of galaxies repeatedly and whenever possible in different nights or runs. Only galaxies with a minimum of 3 independent observations are included in our sample.

We will consider throughout the paper that the *error of the mean* (σ_{mean} , resulting from the repeated measurement of indices in the various galaxy and stellar frames) is:

$$\sigma_{mean} = \frac{s}{\sqrt{N}} \quad (7)$$

with,

$$s = \sqrt{\frac{1}{N-1} \sum_{i=1}^N (x_i - \langle x \rangle)^2} \quad (8)$$

where N is the number of frames per galaxy, x_i is the line-strength measurement in the spectrum i , $\langle x \rangle$ is the mean of the measurements for a galaxy, and s is the standard deviation.

We must emphasize that all error determinations originated from photon counts, spectral noise, etc, are mere error *estimates*; the *measurement* of an error is by definition obtained through repeated experiments. In this work we are presenting data which have the rare advantage of several repeated observations (measurements) per galaxy. On average, to each galaxy we have eight corresponding spectral frames. Therefore, for all the following analysis we will use σ_{mean} as our error.

Finally, for clarity purposes, all the errors presented in this paper (not only for the indices, but for all other measurements) are 1-sigma errors.

4.2 Emission corrections

Emission lines can be seen in many ellipticals at some level. Spectroscopic surveys of early-type galaxies revealed that about 50-60% of the galaxies show weak optical emission lines (Phillips *et al.* 1986; Caldwell 1984). The origin of the gaseous component in ellipticals is not yet understood. It could be either of external origin, for example from a cooling flow or from a merger with a small gas rich galaxy; or it could be of internal origin, resulting from stellar mass loss.

The emission-line spectra of giant elliptical galaxies are usually similar to those of LINERs (Low-Ionization Nuclear Emission Regions), where the ionization is provided by an energetic radiation from the nucleus, usually in the form of a power law. However, Filippenko & Terlevich (1992), Binette *et al.* (1994) and Colina & Arribas (1999) showed that post-AGB stars from the old stellar population of an early-type galaxy can also provide sufficient ionizing radiation to account for the observed H α luminosity and equivalent width.

More important for this study is that stellar absorption line-strength measurements can be affected if there is emission present in the galaxy, which fills the stellar absorptions. In particular, the Balmer line indices used for age-

dating stellar populations can be severely affected if there is emission, leading to wrong age estimates. González (1993) proposed an empirical emission correction for H β using the equivalent width of the emission line [O III] $\lambda 5007$ ($\Delta H\beta = 0.6 \times [\text{O III}] \lambda 5007$, as in Trager *et al.* 2000a). This turns out to be a very insecure correction because the emission spectra of H II regions are strong in H I recombination lines, but the strength of [O III] $\lambda 4959$ and [O III] $\lambda 5007$ lines can greatly differ (Osterbrock 1989; Carrasco *et al.* 1996). We note however, that on average González corrections are shown to be appropriate (Trager *et al.* 2000a).

Unfortunately, most early-type galaxies that show signs of emission lines are discarded from further spectral analysis in the literature, due to small wavelength coverage of the data (i.e. emission lines important to estimate corrections are not available) or the lack of a reliable emission correction technique. Our OAGH spectra instead, with the availability of the H α line information, allow us to use a direct method for emission correction.

In our sample, of the 64 galaxies showing some emission, 29 have a final H β correction > 0.2 Å. Twelve galaxies (NGC 2911 and NGC 3941 classified as Seyferts and 10 LINERs) have been corrected using the H α emission correction.

Table 5 presents the emission-line index definitions used here for H α , [N II] $\lambda 6584$ and [O III] $\lambda 5007$. These definitions work exactly as those of the Lick indices, with a central bandpass flanked by two pseudocontinua.

4.2.1 Balmer lines

Balmer line indices sense mainly the temperature of the turn off point from the main sequence and thus allow an age estimate of the integrated stellar population (e.g., Buzzoni *et al.* 1994). Note that the turn off temperature is also a function of metallicity and therefore the strength of the Balmer absorption is not only a function of age but also a function of metallicity (although to a smaller degree). In reality, the behaviour of Balmer lines at high metallicities seems to be uncertain. For example, Gregg (1994) found, analysing a sample of globular clusters, that the strength of the Balmer lines is only poorly correlated with metallicity above [Fe/H] = -0.7. There are some concerns that stars from other evolutionary phases (e.g., horizontal branch, HB) might contribute significantly to the Balmer absorption. A study of globular clusters by de Freitas Pacheco & Barbuy (1995) showed that blue HB stars may give a substantial contribution to the H β absorption (note that the higher order Balmer lines are more strongly affected by HB-contribution than H β ; e.g., Peterson *et al.* 2003). Furthermore, they suggest that the HB morphology is correlated with the degree of central concentration in the globular cluster. Whether elliptical galaxies are subject to these effects is not yet known. Maraston & Thomas (2000) have attempted to model the effect of HB morphology by calibrating the Balmer indices with globular cluster sample from Burstein *et al.* (1984), Covino *et al.* (1995) and Trager *et al.* (1998). In Maraston *et al.* (2003) it can be appreciated a good consistency between Balmer-line indices from models and observations. It is essential, however, to firstly correct the emission contamination in the Balmer indices before applying model predictions. Widely used in the literature, we are particularly interested in the H β index.

Table 5. Emission index definitions.

Index	Central bandpass	Pseudocontinua
[O III] $\lambda 5007$	4998.000–5015.000	4978.000–4998.000 5015.000–5030.000
H α	6558.000–6568.000	6372.000–6415.000 $\lambda_{red} = 6620.000$
[N II] $\lambda 6584$	6574.000–6594.000	6372.000–6415.000 $\lambda_{red} = 6620.000$

Note: We have assumed that the averaged flux calculated in the blue pseudocontinua for H α and [N II] is equal to the averaged flux in the red continua, because in general the spectra did not have enough wavelength coverage to measure the red pseudocontinua for H α and [N II]. The central wavelength in the red used for the computation of equivalent widths was 6620 Å.

Although the H β index is potentially a good age indicator, is the Balmer line more affected by the presence of nebular emission after H α , and if not corrected will cause a galaxy to appear older than it really is.

As our wavelength range covers the H α line, we have corrected H β using EC(H β) (which stands for Emission Correction of the H β index):

$$EC(H\beta) = \frac{1}{y} \cdot \frac{C_\alpha}{C_\beta} \cdot [EW(H\alpha)_{tot} - EW(H\alpha)_{abs}] \quad (9)$$

where

$$C_\alpha = \frac{Cont(H\alpha)}{\Delta\lambda_\alpha} \quad \text{and} \quad C_\beta = \frac{Cont(H\beta)}{\Delta\lambda_\beta}. \quad (10)$$

Eq. 9 was derived assuming the following simplified definition for equivalent width:

$$EW(\lambda)_{tot} = \left(1 - \frac{F(\lambda)_{tot}}{Cont(\lambda)} \right) \Delta\lambda, \quad (11)$$

where

$$F(\lambda)_{tot} = F(\lambda)_{em} + F(\lambda)_{abs} \quad (12)$$

and

$$F(H\alpha)_{em} = y \times F(H\beta)_{em}. \quad (13)$$

Cont(H α) and Cont(H β) are the continua calculated for H α and H β indices respectively. We assumed $y = 2.85$ for most galaxies (Osterbrock 1989, Case B of recombination, low density limit at electron temperature of 10^4 K). In the equations above, the subscript *tot* stands for total observed values, *em* and *abs* are emission and absorption, respectively. EC(H β) is the emission correction in Ångströms for H β . We have assumed $EW(H\alpha)_{abs} = 1.03 \pm 0.08$ Å[†], derived from EW(H α) measurements in our sample of mainly K stars. Note that the uncertainty in $EW(H\alpha)_{abs}$ takes into account how much a reasonable range of values for $EW(H\alpha)$ in absorption would change the correction.

[†] ± 0.08 represents the peak to peak range of measurements. Ideally this value should be obtained also from spectral synthesis simulations but there is no simulation yet published with resolution high enough at H α to do this estimate.

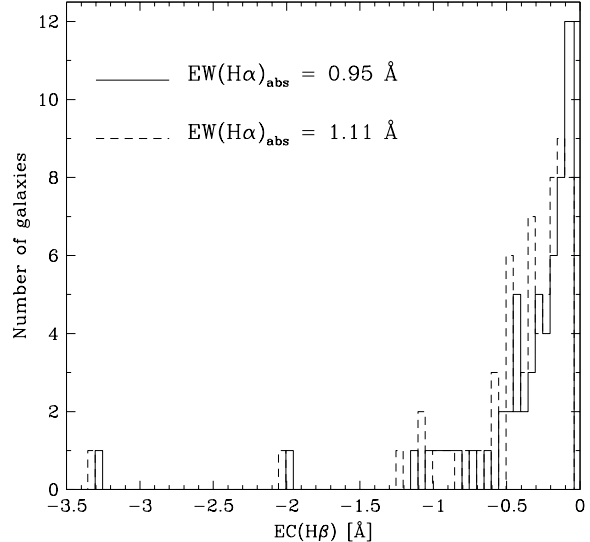


Figure 3. Histogram of emission correction EC(H β) assuming two different values for $EW(H\alpha)_{abs}$. When we take $EW(H\alpha)_{abs} = 0.95$ Å the emission correction is in general less than 0.1 Å smaller than for $EW(H\alpha)_{abs} = 1.11$ Å. The average value for $EW(H\alpha)_{abs}$ used throughout the paper is 1.03 ± 0.08 Å.

We have corrected the Balmer lines using the term EC(H β). The actual correction has been applied to all but 9 galaxies, for which the correction calculated is very small and consistent with zero, and the errors of the correction are larger than the correction itself.

In Figure 3 we show how much the emission correction from eq. 9 would change if we assumed $EW(H\alpha)_{abs} = 0.95$ Å or $EW(H\alpha)_{abs} = 1.11$ Å. The difference in the emission correction for both $EW(H\alpha)_{abs}$ values is generally smaller than 0.1 Å. But this difference is for an extreme variation of $EW(H\alpha)_{abs}$ and must be regarded as an upper limit.

In the expressions above, emission is considered to be negative and absorption positive, therefore $|EC(H\beta)|$ should be subtracted from $EW(H\beta)_{tot}$. In an attempt to compensate for reddening effects in eq. 9, we have assumed a value of 3.0 for the ratio of intensities $F(H\alpha)_{em}/F(H\beta)_{em}$ of a few dusty galaxies: NGC 2872, NGC 3226, NGC 4125, NGC 4494, NGC 5812, NGC 5813 and NGC 5846 (e.g. Forbes 1991, Tran *et al.* 2001). The emission correction to H β using the H α line is presented in column 2 of Table 6.

Trager *et al.* (2000a) have corrected the H β data for emission by subtracting $0.6 \times [\text{O III}] \lambda 5007$ emission to the H β index. This empirical correction is believed to be valid only in a statistical sense, and not accurate for individual galaxies. For comparative purposes, we have measured the [O III] index as defined in Kuntschner *et al.* (2001) and derived the associated emission correction, which is listed in column 3 of Table 6.

Comparing the different emission corrections, the H α and the empirical [O III] $\lambda 5007$ corrections, the difference is small for the majority of galaxies that show emission in the [O III] $\lambda 5007$ forbidden line (see Figure 4-c). We emphasize that it is very dangerous to rely on the [O III] $\lambda 5007$ alone because of the uncertainties in the ionization parameter (i.e., one should not assume the same [O III]/H β ratio for

all galaxies). In principle, the H α -based emission correction has less uncertainties than using [O III] $\lambda 5007$. Note that the errors for the [O III] correction in Table 6 are only the propagation of the error from the repeated measurements of the emission line [O III] $\lambda 5007$: further errors are expected since the [O III] $\lambda 5007/H\beta$ ratio may vary greatly from galaxy to galaxy.

Figure 4 shows the difference between the two emission correction methods for H β . Panels (a) and (b) demonstrate the effects of the emission correction in the H β vs [MgFe] plane. Panel (c) compares the H β index derived from the [O III] (i.e., H β +EC_[O III]) and H α -based (i.e., H β +EC_{H α}) corrections. The H α -based correction (EC_{H α}) is larger than the [O III] one for most cases, the difference can be up to $\sim 1.0 \text{ \AA}$.

Panel (d) shows the comparison between our measurements of [O III] and the values in Trager *et al.* (2000a). The agreement is generally good if we consider the error bars. Note however that we are using an index definition to measure [O III] (Table 5) whereas Trager *et al.* (2000a, T00a) did not use the same definition. The data analysed in T00a is actually a compilation of the data of González (1993), where only the emission profile of the [O III] line was measured.

For the standard elliptical NGC 3379, the H β line index was found to be $1.33 \pm 0.09 \text{ \AA}$ (no emission correction in this value) by Kuntschner (1998), whereas we measure H $\beta = 1.40 \pm 0.06 \text{ \AA}$ (raw value without emission correction). We have measured an emission correction of $0.10 \pm 0.08 \text{ \AA}$ using the H α method, and Kuntschner detected $\sim 0.12 \text{ \AA}$ emission correction for NGC 3379 (using $0.6 \times [\text{O III}] \lambda 5007$).

The other Balmer-line indices, H γ and H δ , were also corrected using the same procedure as in eq. 9, but assuming $y_\gamma = 2.85/0.468 \simeq 6.09$ or $y_\delta = 2.85/0.259 \simeq 11.00$ for F(H α)_{em}/F(H γ)_{em} or F(H α)_{em}/F(H δ)_{em} ratios, respectively (Osterbrock 1989; Case B of recombination, for electron density $n_e < 10^3$ and $T_{eff} = 10^4 \text{ K}$), and changing Cont(H β) for Cont(H γ) or Cont(H δ) accordingly.

The galaxies NGC 1045 and NGC 1453, for which our spectra do not cover the H α line, have been emission corrected for H β using the $0.6 \times [\text{O III}] \lambda 5007$ approximation. In the same way, H $\gamma_{A,F}$ and H $\delta_{A,F}$ for these galaxies have been corrected by the approximated scalings $0.36 \times [\text{O III}]$ and $0.22 \times [\text{O III}]$, respectively, adopted in Kuntschner *et al.* (2002).

4.2.2 Fe5015

Emission can also occur in one of the side-bands of the Lick/IDS indices and raise the continuum which in turn gives larger index values. As pointed out by Kuntschner *et al.* (2002), the Fe5015 index is affected by [O III] $\lambda 5007$ emission in its central bandpass, and by [O III] $\lambda 4959$ emission in its blue continuum bandpass. These authors have derived a correction to Fe5015 by artificially adding spectral emission and examining the effects on the Fe5015 index. We have used their result, where the index can be corrected by adding $+0.61(\pm 0.01) \times [\text{O III}] \lambda 5007$ to the Fe5015 measurement. This procedure has large uncertainties and therefore Fe5015 measurements in ellipticals that show emission, either in H α or [O III], should be considered with care.

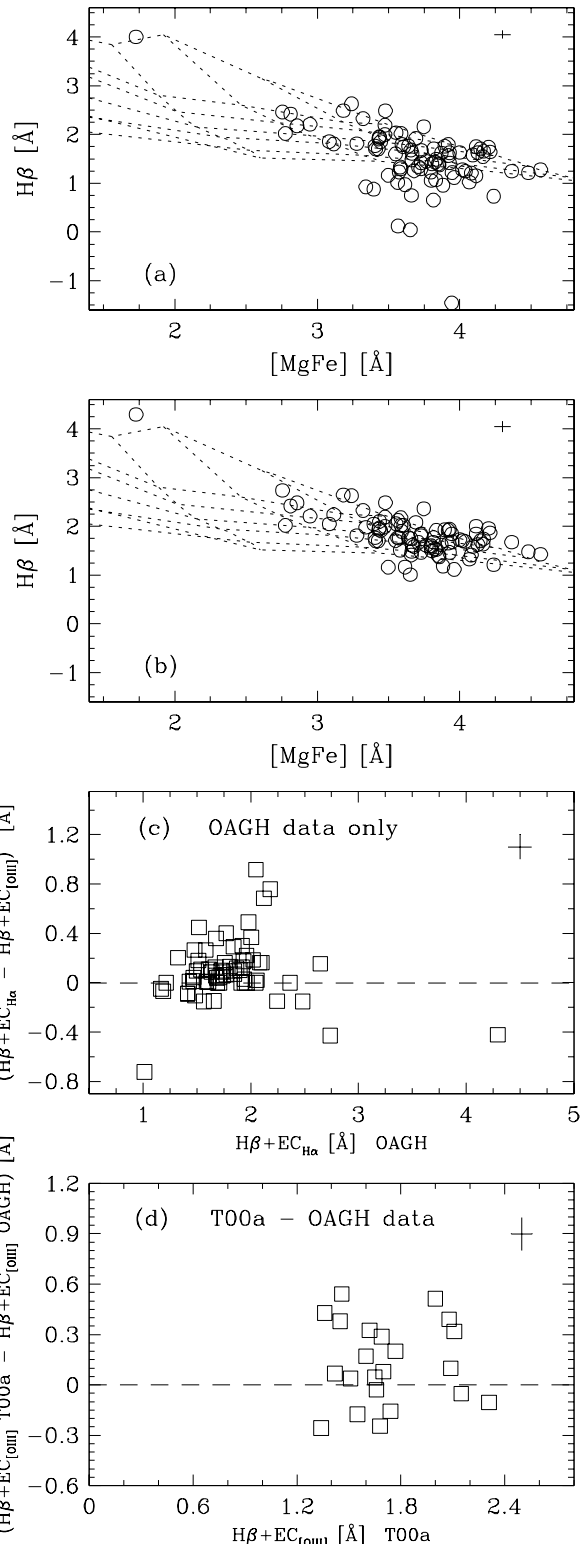


Figure 4. Panels (a) and (b) demonstrate the effect of emission correction in the H β vs [MgFe] plane: (a) no correction, (b) EC(H β) correction applied (Table 6). The dotted lines are single-star population models from Thomas *et al.* (2003) for a range of ages and metallicities. Panel (c) compares the H β index derived with the [O III] and H α -based corrections. Panel (d) presents the comparison between our measurements of [O III] $\lambda 5007$ and the values in Trager *et al.* (2000a, T00a). The error bars on the top right corner of the plots are averages of the error of the mean.

Table 6. Emission corrections in Ångstroms for the galaxies with detected emission lines in the central $r_e/8$ aperture extractions.

Galaxy (1)	EC(H β) (2)	$0.6 \times [\text{O III}] \lambda 5007$ (3)	EW(H α) $_{tot}$ (4)	EW([N II] $\lambda 6584$) (5)	EC(H γ_A) (6)	EC(H δ_A) (7)
NGC 0315	-0.85 ± 0.09	-0.48 ± 0.16	-1.01 ± 0.02	—	-0.71 ± 0.11	-0.50 ± 0.11
NGC 0474	-0.11 ± 0.08	-0.06 ± 0.06	0.77 ± 0.04	—	—	—
NGC 0584	-0.10 ± 0.08	—	0.79 ± 0.01	-0.29 ± 0.02	—	—
NGC 0720	-0.09 ± 0.08	—	0.82 ± 0.02	—	—	—
NGC 0821	-0.13 ± 0.08	—	0.71 ± 0.05	-0.23 ± 0.08	—	—
NGC 1045	*	-0.32 ± 0.08	*	*	*	*
NGC 1052	-3.30 ± 0.40	-3.23 ± 0.09	-6.89 ± 0.20	-12.22 ± 0.18	-2.75 ± 0.52	-1.95 ± 0.54
NGC 1407	-0.22 ± 0.07	—	0.50 ± 0.03	-0.13 ± 0.01	—	—
NGC 1453	*	-0.48 ± 0.08	*	*	*	*
NGC 1600	-0.23 ± 0.07	-0.11 ± 0.10	0.49 ± 0.04	-0.23 ± 0.10	—	—
NGC 1700	-0.16 ± 0.08	—	0.64 ± 0.01	-0.52 ± 0.01	—	—
NGC 1726	-0.33 ± 0.09	-0.21 ± 0.12	0.23 ± 0.15	-0.87 ± 0.15	—	—
NGC 2128	-1.17 ± 0.12	-0.25 ± 0.10	-1.78 ± 0.05	-3.88 ± 0.03	-0.97 ± 0.16	-0.69 ± 0.16
NGC 2300	-0.07 ± 0.09	—	0.88 ± 0.05	-0.38 ± 0.12	—	—
NGC 2418	-0.47 ± 0.07	-0.43 ± 0.06	-0.09 ± 0.04	-1.36 ± 0.04	-0.39 ± 0.08	-0.28 ± 0.08
NGC 2513	-0.09 ± 0.09	—	0.82 ± 0.07	—	—	—
NGC 2549	-0.20 ± 0.13	-0.20 ± 0.13	1.26 ± 0.01	—	—	—
NGC 2768	-0.55 ± 0.07	-0.54 ± 0.11	-0.29 ± 0.05	-1.59 ± 0.07	-0.46 ± 0.09	-0.33 ± 0.09
NGC 2872	-0.11 ± 0.09	—	0.77 ± 0.08	-0.16 ± 0.08	—	—
NGC 2911	-2.00 ± 0.23	-1.32 ± 0.14	-3.77 ± 0.13	-9.55 ± 0.18	-1.66 ± 0.29	-1.18 ± 0.31
NGC 2974	-0.66 ± 0.08	-0.75 ± 0.09	-0.56 ± 0.02	-3.40 ± 0.11	-0.55 ± 0.09	-0.39 ± 0.09
NGC 3091	-0.15 ± 0.08	-0.14 ± 0.08	0.67 ± 0.06	—	—	—
NGC 3098	-0.19 ± 0.11	-0.19 ± 0.11	1.35 ± 0.01	—	—	—
NGC 3115	-0.10 ± 0.08	—	0.80 ± 0.03	—	—	—
NGC 3139	-0.03 ± 0.09	—	0.95 ± 0.05	—	—	—
NGC 3156	-0.29 ± 0.09	-0.71 ± 0.07	0.33 ± 0.13	-0.96 ± 0.02	—	—
NGC 3193	-0.09 ± 0.08	-0.24 ± 0.01	0.81 ± 0.03	—	—	—
NGC 3226	-0.97 ± 0.10	-1.69 ± 0.05	-1.29 ± 0.02	-2.86 ± 0.13	-0.80 ± 0.13	-0.57 ± 0.13
NGC 3245	-0.75 ± 0.08	-0.35 ± 0.07	-0.78 ± 0.02	-1.64 ± 0.12	-0.63 ± 0.10	-0.45 ± 0.10
NGC 3377	-0.01 ± 0.04	-0.01 ± 0.04	1.37 ± 0.02	—	—	—
NGC 3379	-0.10 ± 0.08	—	0.80 ± 0.03	—	—	—
NGC 3414	-1.02 ± 0.11	-0.96 ± 0.07	-1.42 ± 0.06	-3.42 ± 0.08	-0.85 ± 0.13	-0.60 ± 0.14
NGC 3599	-0.28 ± 0.08	-0.70 ± 0.02	0.37 ± 0.07	-1.60 ± 0.13	—	—
NGC 3607	-0.43 ± 0.07	-0.13 ± 0.01	0.01 ± 0.01	-2.21 ± 0.02	—	—
NGC 3608	-0.16 ± 0.08	-0.06 ± 0.08	0.64 ± 0.03	-0.19 ± 0.04	—	—
NGC 3613	-0.06 ± 0.09	—	0.88 ± 0.06	—	—	—
NGC 3636	-0.06 ± 0.05	-0.06 ± 0.05	1.14 ± 0.11	—	—	—
NGC 3640	-0.02 ± 0.09	—	0.98 ± 0.04	—	—	—
NGC 3665	-0.88 ± 0.09	-0.13 ± 0.01	-1.09 ± 0.02	-1.15 ± 0.05	-0.74 ± 0.11	-0.52 ± 0.12
NGC 3923	-0.13 ± 0.08	—	0.73 ± 0.02	—	—	—
NGC 3941	-0.28 ± 0.07	-0.09 ± 0.11	0.37 ± 0.02	-0.56 ± 0.04	—	—
NGC 4125	-0.53 ± 0.07	-0.37 ± 0.20	-0.23 ± 0.04	-2.64 ± 0.10	-0.44 ± 0.08	-0.31 ± 0.09
NGC 4261	-0.21 ± 0.08	-0.29 ± 0.05	0.54 ± 0.08	-1.44 ± 0.10	—	—
NGC 4365	-0.10 ± 0.08	—	0.80 ± 0.02	—	—	—
NGC 4374	-0.55 ± 0.08	-0.25 ± 0.03	-0.28 ± 0.07	-1.63 ± 0.04	-0.45 ± 0.09	-0.32 ± 0.09
NGC 4550	-0.44 ± 0.08	-0.59 ± 0.09	-0.02 ± 0.11	-0.27 ± 0.08	-0.36 ± 0.09	-0.26 ± 0.09
NGC 4754	-0.01 ± 0.09	—	1.01 ± 0.04	—	—	—
NGC 5322	-0.16 ± 0.08	—	0.64 ± 0.02	-0.50 ± 0.02	—	—
NGC 5353	-0.43 ± 0.07	-0.07 ± 0.06	0.01 ± 0.04	-1.42 ± 0.10	—	—
NGC 5354	-0.19 ± 0.08	-0.24 ± 0.12	0.57 ± 0.03	-0.14 ± 0.08	—	—
NGC 5363	-1.05 ± 0.11	-0.56 ± 0.05	-1.50 ± 0.06	-3.12 ± 0.02	-0.88 ± 0.14	-0.62 ± 0.14
NGC 5444	-0.23 ± 0.08	-0.29 ± 0.06	0.49 ± 0.05	-0.42 ± 0.10	—	—
NGC 5813	-0.33 ± 0.07	-0.06 ± 0.06	0.25 ± 0.05	-0.77 ± 0.14	—	—
NGC 5831	-0.05 ± 0.09	-0.03 ± 0.10	0.92 ± 0.07	—	—	—
NGC 5845	-0.17 ± 0.08	—	0.61 ± 0.05	-0.31 ± 0.05	—	—
NGC 5846	-0.45 ± 0.07	—	-0.05 ± 0.03	-1.82 ± 0.08	-0.37 ± 0.08	-0.27 ± 0.08
NGC 5846A	-0.01 ± 0.09	-0.11 ± 0.04	1.02 ± 0.03	—	—	—
NGC 5869	-0.33 ± 0.51	-0.33 ± 0.51	1.14 ± 0.06	—	—	—
NGC 5982	-0.04 ± 0.09	—	0.93 ± 0.01	—	—	—
NGC 6172	-0.30 ± 0.07	-0.46 ± 0.10	0.30 ± 0.04	-1.74 ± 0.08	—	—
NGC 7302	-0.03 ± 0.09	—	0.96 ± 0.08	-0.29 ± 0.06	—	—
NGC 7585	-0.16 ± 0.08	—	0.66 ± 0.02	-1.19 ± 0.09	—	—
NGC 7619	-0.27 ± 0.07	—	0.40 ± 0.03	-0.33 ± 0.05	—	—
NGC 7626	-0.30 ± 0.07	-0.10 ± 0.07	0.31 ± 0.03	—	—	—

Notes: EC(λ) was derived using $\text{EW}(\text{H}\alpha)_{abs} = 1.03$ Å (see eq. 9). The * symbol is used when H α and/or [N II] fell outside the wavelength limits of the spectra and could not be measured. The — symbol denotes no emission component detected (if EC(H β) shows — it is because no emission was detected in H α). The negative signs denote emission, therefore, the EC(λ) corrections must be subtracted from the effective index measurement, e.g., $H\beta_{correct} = H\beta - \text{EC}(H\beta)$. Columns 4 and 5 are EW(H α) and EW([N II]) indices, measured in Ångstroms, and defined in Table 5.

5 KINEMATICS

Estimates of the galaxy central velocity dispersion σ_0 and radial velocity were derived with the **IRAF** task **fxcor**. This program uses the cross-correlation method to measure the redshift of the galaxy spectra. A comparison between our redshift determination and that taken from **NED** is presented in Figure 5-a. Simultaneously, the measured width (FWHM) of the correlation peak is used to estimate the velocity dispersion ($\text{FWHM} = 2\sqrt{\ln 4}\sigma$). The width of the peak will be related to the broadening of the galaxy absorption lines compared to the instrumental resolution of the template star, i.e., $\text{FWHM}_{fxcor}^2 = \text{FWHM}_{galaxy}^2 + \text{FWHM}_{template}^2$.

Within the **fxcor** task the spectra of galaxy and template are continuum subtracted and cut to a user defined wavelength range (4350-5250 [Å] and 5300-6200 [Å], for the blue and red observations respectively). Then cross-correlation is performed in the Fourier space, and a “square” filter is applied to remove large scale variations as well as noise from the spectra. The instrumental dispersion of the OAGH observations is approximately $100 \text{ km s}^{-1} \text{ pixel}^{-1}$ for the blue region and $80 \text{ km s}^{-1} \text{ pixel}^{-1}$ for the red region[†]. Multiple measurements of the same galaxy were averaged. We have adopted the error of the mean as our final velocity dispersion error (equation 7).

We note that the H β feature, present in one of the wavelength intervals, is known to be a source for severe template mismatch for galaxies with strong Balmer absorption (Kuntschner 1998, 2000). Indeed we find some galaxies in our sample with very strong H β feature, i.e., $H\beta > 2.5 \text{ Å}$ (NGC 3156 has $H\beta \simeq 3.5 \text{ Å}$). For the same reason, we also have opted to exclude the H γ feature from our velocity dispersion measurements. The red wavelength interval on the other hand, encompasses the NaD band, which has an important contribution from interstellar absorption (Dressler 1984). To avoid these template mismatch and contamination problems without losing important information from other wavelengths, we have removed the H β and NaD features from the template spectra used for the cross-correlation. This way, the weight of the H β and NaD regions during the cross-correlation in the Fourier space is kept lower in comparison to any of the other intense correlation features (e.g., the Mg triplet).

Figure 5 presents the comparison between our kinematical measurements and the literature. In panel (a) we see a good agreement (inside the errors) of our radial velocities and values obtained from NED. To do this comparison we have selected in NED the most recent radial velocities derived from optical spectroscopy. In Figure 5-b we show a comparison between our estimated central velocity dispersion and the mean scaled σ_0 in the compilation by Prugniel & Simien (1996, PS96). In order to compare our measurements with literature values, we have corrected σ_0 to a standard aperture as described by Jørgensen, Franx & Kjaergaard (1995), which scales σ to a normalized diameter

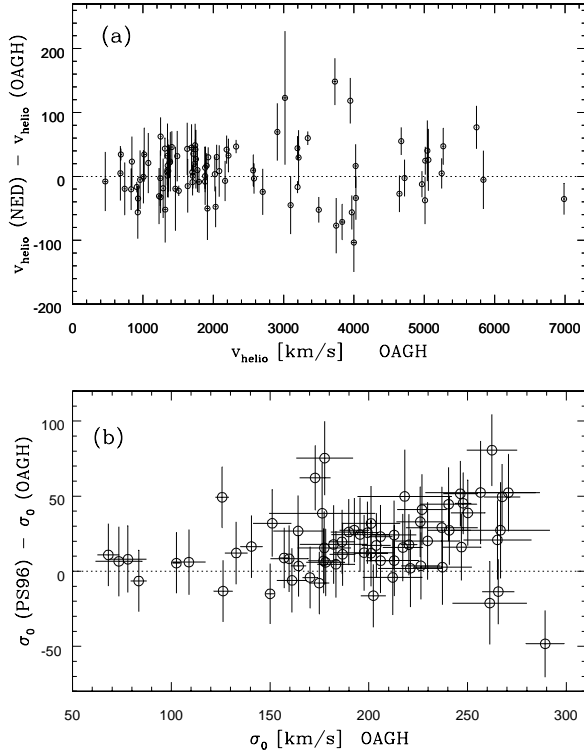


Figure 5. (a) Comparison between our measured radial velocities and published values. (b) Comparison of our measured central velocity dispersions with the σ_0 from the compilation of Prugniel & Simien (1996, PS96). The average error bar adopted for the PS96 compilation is 20 km/s.

equivalent to 3.4 arcsec projected on to a galaxy in the Coma cluster. This correction is generally $< 10 \text{ km/s}$ for our sample. The results agree with those in the literature on a 70% level, using a Kolmogorov-Smirnov test. For galaxies showing $\sigma_0 \lesssim 100 \text{ km/s}$, systematic errors start to dominate as our spectral resolution is lower than the measurement, and therefore these low velocity dispersions should be considered only as rough estimates. Note that there is a small offset in Figure 5-b, our σ_0 is on average 16 km/s smaller than in PS96. For NGC 3379, we obtain $\sigma_0 = 203 \pm 7 \text{ km/s}$; Davies *et al.* (1987) find $201 \pm 20 \text{ km/s}$; Franx *et al.* (1989): $220 \pm 3 \text{ km/s}$; Tonry & Davis (1981): $214 \pm 15 \text{ km/s}$; Bender *et al.* (1994): $240 \pm 5 \text{ km/s}$; and the average value adopted by Prugniel & Simien (1996) for the compilation of 17 results on NGC 3379 is 221 km/s . We estimate the average uncertainty in the PS96 compilation to be at least of the order of 20 km/s from the multiple measurements, whereas our mean error bar is 11 km/s (or in logarithmic scale, our mean error is 0.024 in σ). Thus, we do not regard as important the offset between our data and the PS96 compilation.

Table 7 lists the adopted radial velocities and aperture re-scaled central velocity dispersions for our galaxy sample.

[†] Note that to measure Lick indices and compare with literature data and models we have to degrade the resolution of the spectra to the values in Table 4. However, to measure velocity dispersion and radial velocity we have used our original observations where no smoothing of the data was performed.

Table 7. Measured radial velocities (v_{helio}) and central velocity dispersions (σ_0) scaled to a standard circular aperture (see text, Section 5).

Galaxy	v_{helio} [km/s]	σ_0 [km/s]	Galaxy	v_{helio} [km/s]	σ_0 [km/s]
ESO 462-G015	5840 ± 27	239 ± 24	NGC 3599	832 ± 9	68 ± 5
MCG -01-03-018	5743 ± 10	191 ± 14	NGC 3607	960 ± 20	221 ± 16
NGC 0016	3100 ± 17	151 ± 9	NGC 3608	1229 ± 12	182 ± 16
NGC 0221	-123 ± 10	83 ± 4	NGC 3610	1704 ± 11	174 ± 5
NGC 0315	4968 ± 11	246 ± 8	NGC 3613	2034 ± 15	205 ± 7
NGC 0474	2325 ± 7	159 ± 9	NGC 3636	1741 ± 13	127 ± 3
NGC 0584	1883 ± 11	199 ± 5	NGC 3640	1251 ± 12	178 ± 9
NGC 0720	1725 ± 9	261 ± 18	NGC 3665	2049 ± 10	202 ± 6
NGC 0750	5248 ± 16	189 ± 9	NGC 3923	1796 ± 13	289 ± 9
NGC 0751	5270 ± 15	186 ± 6	NGC 3941	926 ± 9	125 ± 3
NGC 0777	5015 ± 8	267 ± 9	NGC 4125	1347 ± 35	201 ± 14
NGC 0821	1717 ± 11	212 ± 15	NGC 4261	2191 ± 11	256 ± 27
NGC 0890	4027 ± 26	205 ± 5	NGC 4365	1248 ± 14	236 ± 18
NGC 1045	4646 ± 9	230 ± 16	NGC 4374	1007 ± 14	247 ± 4
NGC 1052	1510 ± 6	176 ± 26	NGC 4494	1344 ± 11	161 ± 7
NGC 1132	6988 ± 17	237 ± 14	NGC 4550	465 ± 21	73 ± 11
NGC 1407	1774 ± 19	265 ± 17	NGC 4754	1347 ± 9	186 ± 6
NGC 1453	3999 ± 28	250 ± 8	NGC 5322	1754 ± 16	217 ± 10
NGC 1600	4720 ± 17	262 ± 12	NGC 5353	2169 ± 16	266 ± 25
NGC 1700	3971 ± 13	220 ± 4	NGC 5354	2579 ± 13	208 ± 8
NGC 1726	4025 ± 24	212 ± 11	NGC 5363	1077 ± 9	175 ± 33
NGC 2128	3019 ± 30	178 ± 10	NGC 5444	3948 ± 10	212 ± 12
NGC 2300	1905 ± 7	265 ± 8	NGC 5557	3213 ± 18	226 ± 12
NGC 2418	5043 ± 7	240 ± 10	NGC 5576	1487 ± 6	183 ± 9
NGC 2513	4672 ± 13	246 ± 9	NGC 5638	1637 ± 11	157 ± 4
NGC 2549	1019 ± 14	140 ± 5	NGC 5812	1885 ± 13	201 ± 8
NGC 2768	1360 ± 6	177 ± 13	NGC 5813	1929 ± 7	226 ± 9
NGC 2872	3196 ± 11	240 ± 14	NGC 5831	1629 ± 8	164 ± 3
NGC 2911	3199 ± 7	172 ± 7	NGC 5845	1410 ± 22	200 ± 14
NGC 2974	1916 ± 23	197 ± 15	NGC 5846	1708 ± 17	219 ± 14
NGC 3091	3729 ± 17	285 ± 22	NGC 5846A	2217 ± 16	183 ± 8
NGC 3098	1387 ± 13	108 ± 8	NGC 5854	1691 ± 35	135 ± 4
NGC 3115	685 ± 7	218 ± 23	NGC 5864	1885 ± 4	130 ± 5
NGC 3139	1412 ± 10	184 ± 9	NGC 5869	2085 ± 4	162 ± 18
NGC 3156	1318 ± 16	78 ± 9	NGC 5982	2911 ± 22	229 ± 16
NGC 3193	1377 ± 18	220 ± 20	NGC 6172	5009 ± 8	136 ± 6
NGC 3226	1287 ± 11	164 ± 12	NGC 6411	3747 ± 16	177 ± 7
NGC 3245	1314 ± 6	192 ± 7	NGC 7302	2703 ± 16	188 ± 7
NGC 3377	679 ± 17	132 ± 5	NGC 7332	1250 ± 16	150 ± 4
NGC 3379	912 ± 6	203 ± 7	NGC 7454	2022 ± 5	126 ± 4
NGC 3384	740 ± 15	170 ± 3	NGC 7585	3499 ± 14	195 ± 14
NGC 3412	844 ± 10	102 ± 4	NGC 7619	3833 ± 27	270 ± 16
NGC 3414	1460 ± 23	177 ± 14	NGC 7626	3345 ± 9	226 ± 12

tral features, in general reducing the observed line-strength compared to intrinsic values. In fact, it is well known that there is a velocity dispersion dependence on the indices and it needs to be corrected (e.g., González 1993; Jørgensen *et al.* 1995). In order to compare the raw index measurements in galaxies with the model predictions we calibrate the indices to zero velocity dispersion. The procedure adopted here is to broaden the spectra of template stars with gaussians of $\sigma_0 = 20\text{--}400$ km/s in bins of 20 km/s. The indices are then measured for each σ bin and a correction factor is determined. The correction factor has the form $C(\sigma) = \text{index}(\sigma=0)/\text{index}(\sigma)$ for indices measured in Ångstroms, and $C(\sigma) = \text{index}(\sigma=0) - \text{index}(\sigma)$ for indices given in magnitudes. It is important to stress that derived correction factors are only useful if the stars used for the simulations resemble the galaxy spectra. For this reason, we have opted to

build a composite stellar spectrum template, and compared the resulting super-template with the spectra of NGC 3379, observed in every run. The super-template was created by averaging different stellar-type spectra selected from Table 3, carefully allocating more weight to the K giant stars. Figure 6 shows the dependence of the correction factor on σ for 25 Lick indices measured in stars; the dotted bars denote the uncertainty range in the correction due to errors in the index measurements. A polynomial fitting to the curves in Figure 6 allowed for the velocity dispersion corrections, which were then added or multiplied (if in units of mag or Å respectively) to the raw index measurements of the resolution corrected galaxy spectra. In this procedure, the errors in σ_0 are then propagated to the index errors.

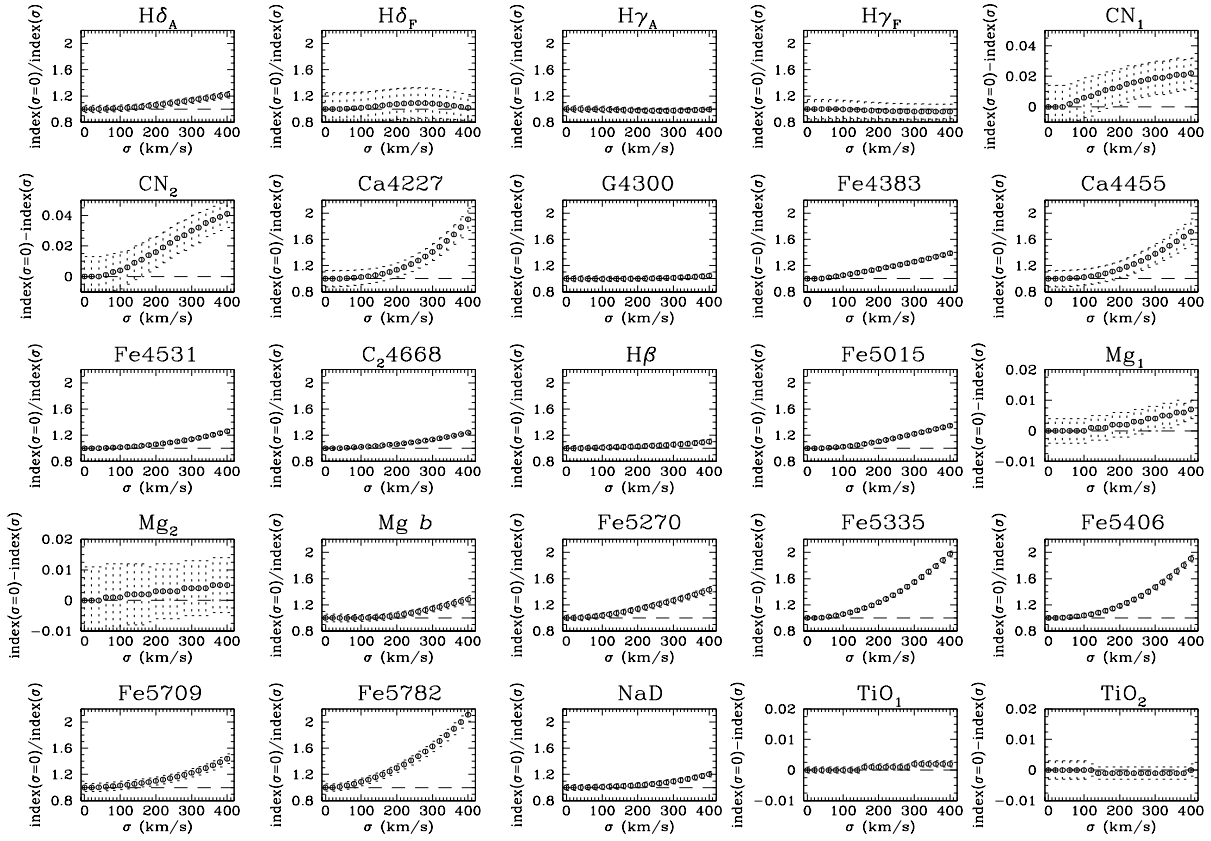


Figure 6. Velocity dispersion corrections. The σ broadening and index measurements were performed on a composite stellar spectrum template that very well matches the spectra of the bona fide elliptical galaxy NGC 3379. The dotted bars represent the uncertainties derived from the index measurement errors. The dashed line is used as a visual guide-line for no correction applied.

6 FINAL CENTRAL ABSORPTION LINE-STRENGTH

To remove any remaining systematic offset between our measurements and the Lick/IDS, we have compared the measurements of 25 line-strength indices of our 45 stars observed in common with Lick. Generally there is good agreement between the two data sets, and only small offsets are found (see Figure 7, for an offset-corrected comparison). The mean offsets and associated errors for each index are summarized in Table 8. These offsets were then applied to our data.

The final corrected central $r_e/8$ index measurements and associated errors for our galaxy sample are presented in the Appendix B in Table B.1.

6.1 Summary: the sample and Lick indices

Trager *et al.* (1998) have demonstrated that index errors can masquerade as real trends in the determination of ages, metallicities and their correlations with velocity dispersion. Here we give special treatment to the H β -index because this index will be used in subsequent papers to infer ages and metallicities, using for example, H β -[MgFe] index diagrams. It happens so that the information on H β errors is commonly used to separate and select the best galaxy data in the literature. The sample used by Trager *et al.* (1998) had a typical error of $\delta H\beta = 0.191 \text{ \AA}$. A reasonable guide is that H β must

Table 8. Lick/IDS offsets.

Index	Offset (Lick/IDS – OAGH)
H δ_A	$-0.07 \pm 0.18 \text{ \AA}$
H δ_F	$-0.09 \pm 0.09 \text{ \AA}$
H γ_A	$+0.16 \pm 0.10 \text{ \AA}$
H γ_F	$+0.18 \pm 0.05 \text{ \AA}$
CN ₁	$0.000 \pm 0.005 \text{ mag}$
CN ₂	$-0.011 \pm 0.006 \text{ mag}$
Ca4227	$-0.04 \pm 0.04 \text{ \AA}$
G4300	$-0.03 \pm 0.08 \text{ \AA}$
Fe4383	$+0.19 \pm 0.09 \text{ \AA}$
Ca4455	$+0.29 \pm 0.05 \text{ \AA}$
Fe4531	$+0.27 \pm 0.08 \text{ \AA}$
C ₂ 4668	$+0.06 \pm 0.10 \text{ \AA}$
H β	$-0.06 \pm 0.04 \text{ \AA}$
Fe5015	$-0.17 \pm 0.08 \text{ \AA}$
Mg ₁	$+0.011 \pm 0.002 \text{ mag}$
Mg ₂	$+0.023 \pm 0.003 \text{ mag}$
Mg _b	$-0.09 \pm 0.05 \text{ \AA}$
Fe5270	$-0.07 \pm 0.04 \text{ \AA}$
Fe5335	$-0.12 \pm 0.05 \text{ \AA}$
Fe5406	$-0.03 \pm 0.03 \text{ \AA}$
Fe5709	$+0.05 \pm 0.03 \text{ \AA}$
Fe5782	$+0.05 \pm 0.02 \text{ \AA}$
NaD	$+0.09 \pm 0.03 \text{ \AA}$
TiO ₁	$+0.006 \pm 0.001 \text{ mag}$
TiO ₂	$+0.002 \pm 0.002 \text{ mag}$

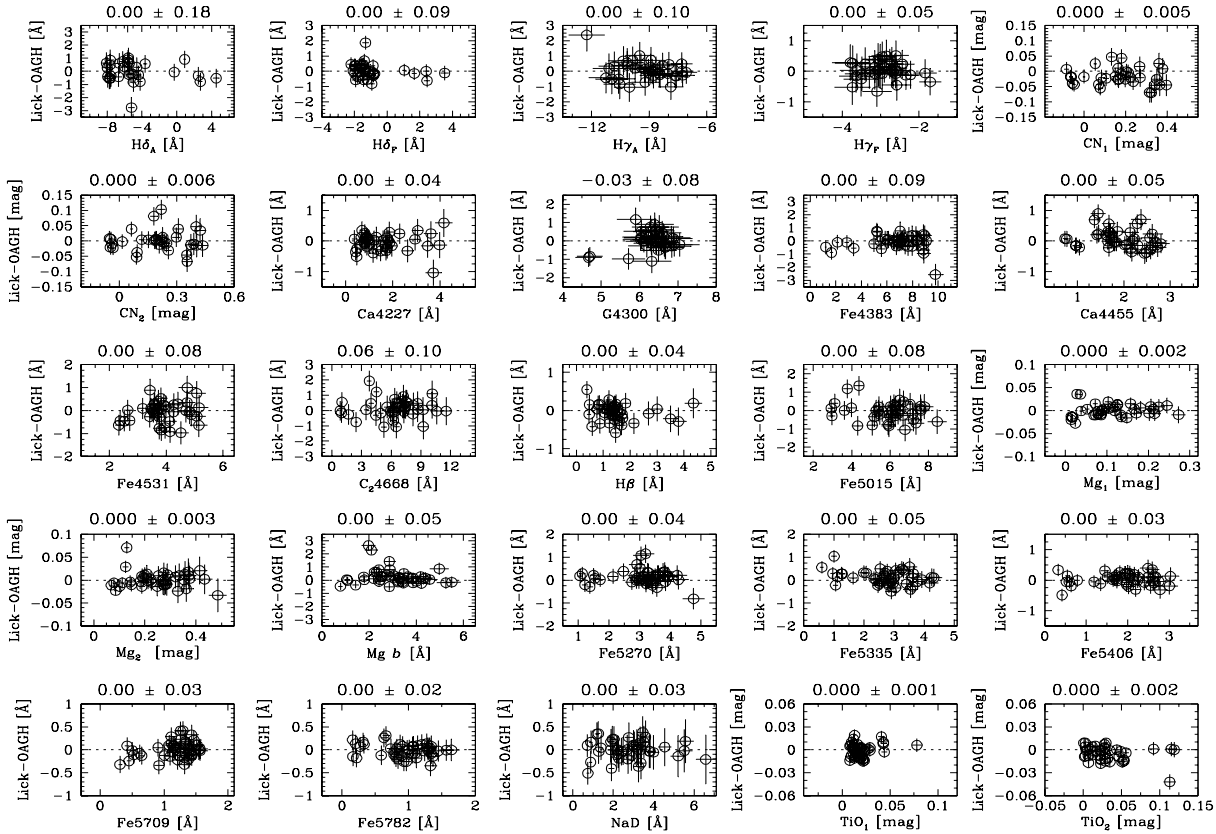


Figure 7. Comparison between our line-strength measurements and Worthey *et al.* (1994) for 45 stars in common. Our data were corrected for the Lick/IDS offset prior to comparison. The remaining offset and associated 1σ error are shown above each mini-plot. The offsets are summarised in Table 8.

be accurate to $\sim 0.1 \text{ \AA}$ in order to determine reliable ages and metallicities.

Figure 8 shows a histogram of $H\beta$ -index errors. These errors take into account the errors in the emission correction, i.e., we have propagated the errors of the emission correction into the new $H\beta_{correct}$ error following eq. 9. The median error of the sample is 0.125 \AA . Previous to the emission correction, the median error of our data was 0.086 \AA .

The errors in the determination of ages and metallicities from index-index diagrams will be addressed again in a subsequent paper.

Our survey has the advantage of covering a large wavelength range, from $\sim 3850 \text{ \AA}$ to 6700 \AA , giving $H\alpha$ information which is important for emission correction. Of the 86 galaxies with $S/N \geq 15$ (for $r_e/8$ aperture, and per resolution element), 52 had $H\beta$ -index corrected for emission, the corrections varied from as small as $\sim 0.1 \text{ \AA}$ to as large as $\sim 3.3 \text{ \AA}$ for NGC 1052; 41 galaxies present $[\text{O III}] \lambda 5007$ emission, of which 16 also show obvious $H\alpha$ emission. Most of the galaxies in the sample do not show obvious signs of disturbances nor tidal features in their morphologies, although 11 galaxies belong to the Arp catalogue of peculiar galaxies (Arp 1966), of which only three (NGC 750, NGC 751 and NGC 3226) seem to be strongly interacting.

We have applied a better method for emission correction of the Balmer-line indices than the use of the uncertain $0.6 \times [\text{O III}]$ estimation. The new correction uses the intensity and equivalent width of the $H\alpha$ index (defined in Table 5).

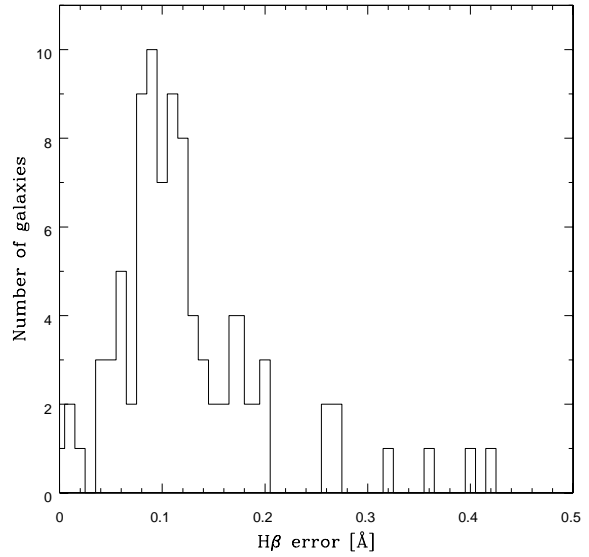


Figure 8. Histogram of $H\beta$ -index errors (error of the mean per galaxy). These uncertainties take into account the errors in the emission correction. The median error of the sample is 0.125 \AA .

We note that nebular emission could still be affecting the ages and metallicities derived from most of the data in the literature.

7 INDEX- σ RELATIONS

In this Section, we will compare $\log \sigma_0$ with indices measured in magnitudes. Indices originally measured in Ångstroms are converted to magnitudes as explained in eq. 4, and now denoted with a prime, i.e., $H\beta$ in magnitudes will be called $H\beta'$.

The dynamical properties of galaxy cores are closely connected with their stellar populations, implied by the relatively small scatter in the colour- σ_0 , Mg- σ_0 relations found in previous investigations (e.g. Terlevich *et al.* 1981, Burstein *et al.* 1988, Bower, Lucey & Ellis 1992). The prominence of the Mg- σ_0 relation suggests that other metal line-strength indices should also exhibit a correlation with the central velocity dispersion. We present in Figures 9 and 10 the index- σ_0 relations for $\langle Fe \rangle'$, CN₁, two Balmer-line indices ($H\beta'$, $H\gamma_A'$), Mg b' and Mg g' .

We have performed ordinary least square fits with $Y = \text{Index}'$, as the dependent variable (hereafter the $(Y|X)$ fit; solid line in Figures 9 and 10) and also a fit in which Index' is the independent variable (dotted line in Figures 9 and 10). Isobe *et al.* (1990) recommend the $(Y|X)$ fit for scientific problems where one variable is clearly an effect and the other the cause. The combination of the regressions of Y on X and X on Y allows us to compute the linear correlation coefficient $R = \sqrt{bb'}$, where $Y = a + bX$ and $X = a' + b'Y$. Here both regressions are shown to illustrate how different fitting methods lead to different results. For the Index'- σ_0 relation analysis, we favour the $(Y|X)$ fit method for two reasons: (1) consistency with previous authors, as frequently they fit their data using the $(Y|X)$ method; (2) at least the Mg content of a galaxy seems to be driven by the central potential of the galaxy (see conclusions of Colless *et al.* 1999) which is approximated by its central velocity dispersion σ_0 . The code used to derive the $(Y|X)$ fits is an **IRAF** implementation of the Fortran code by Bevington (1969). Table 9 presents the $(Y|X)$ fit values and uncertainties for all the sample (Es+S0s).

In Figures 9 and 10 we compare our results with the Fornax cluster sample from Kuntschner (2000; 22 galaxies), and the ‘mixed’ galaxy sample from Kuntschner *et al.* (2001; 72 galaxies), which includes Virgo and Coma clusters galaxies, a few S0s and galaxies in less dense environments. Consistent with the results of Kuntschner (2000) and Kuntschner *et al.* (2001, 2002), we find a weak correlation between the $\langle Fe \rangle$ index and σ_0 . The slope of the $\langle Fe \rangle' - \log \sigma_0$ relation is the smallest in Table 9. The Mg₂- σ_0 and $\langle Fe \rangle' - \log \sigma_0$ relations presented here for group, field and isolated galaxies are not significantly different from those of cluster E/S0s (see fits plotted in Figures 9 and 10). Nonetheless, the slopes of the other relations (except CN₁ - $\log \sigma_0$, which has no comparison) are significantly different with respect to previous authors, even though all relations are still following the trend of increasing metallicity with increasing velocity dispersion.

It is necessary to point out that the shift in the dashed lines between the fit of $\langle Fe \rangle$ and Mg b' indices for K2000 and K2001 in Figures 9(b) and 9(c) is probably related to the fact that, while K2000 are “central” values for the equidistant Fornax cluster galaxies, K2001 values are for a fixed linear aperture as in this paper. We have no explanation for the shift in $\langle Fe \rangle$ indices between K2001 and this work,

Table 10. Kuntschner *et al.* (2000, 2001) least square fit results.

K2000:	
Mg ₂	$-(0.127 \pm 0.054) + (0.191 \pm 0.023) \log \sigma_0$
Mg b'	$-(0.056 \pm 0.044) + (0.102 \pm 0.020) \log \sigma_0$
$\langle Fe \rangle'$	$+(0.015 \pm 0.053) + (0.038 \pm 0.023) \log \sigma_0$
H β'	$+(0.106 \pm 0.015) - (0.020 \pm 0.007) \log \sigma_0$
H γ_A'	$-(0.038 \pm 0.044) - (0.045 \pm 0.019) \log \sigma_0$

K2001:	
Mg b'	$-(0.163 \pm 0.031) + (0.142 \pm 0.013) \log \sigma_0$
$\langle Fe \rangle'$	$-(0.034 \pm 0.015) + (0.021 \pm 0.006) \log \sigma_0$

other than that K2001 includes a more “mixed” sample of galaxies.

The fit values for the Fornax cluster in Kuntschner (2000) and for the field, group and cluster galaxies in Kuntschner *et al.* (2001) are shown in Table 10.

Figures 9-d and 10-a show the index- σ_0 relations for two Balmer-line indices (H β' and H γ_A'). Both indices show negative correlations with the central velocity dispersion. In Figure 10-b, the CN₁ index correlates with σ_0 almost as strongly as Mg₂, however with larger scatter. In a subsequent paper we will discuss the sensitivity of CN indices to α -elements like Mg.

Note that on average most S0 galaxies have slightly lower σ_0 values than the bulk of Es. Remarkably, bulges of S0s follow the same general relation with σ_0 as the elliptical galaxies. Yet, the peculiar S0 galaxy NGC 3156 shows a Mg absorption which is too low by 0.080 and 0.040 mag for Mg₂ and $\langle Fe \rangle'$ respectively. As we will in a subsequent paper, this galaxy has a very young (luminosity weighted) central stellar population for an early-type galaxy of its brightness and velocity dispersion. This may be an extreme case, but it demonstrates nicely how the Mg, Fe, H β , H γ - σ_0 relations can be influenced by young stellar populations in the centre of the galaxy. We also note that the bulk of galaxies in our sample with higher H β and H γ index values (i.e., indicative of younger stellar populations according to single-star population models [forthcoming paper]) have relatively small velocity dispersions. We note also that of the four galaxies with $\log \sigma < 2.0$ in our sample, two are classified as field galaxies (NGC 3599, NGC 4550), and the other two are NGC 221, a compact dwarf elliptical, and NGC 3156, an outlier galaxy in our sample (c.f., Figures 9 and 10).

On average our Mg-absorption strength is lower than in the Fornax galaxies from Kuntschner (2000). This could either be a metallicity or/and age related effect. As we have seen, there is a general trend that the presence of young stellar populations moves galaxies to lower Mg values. Some examples of anomalously low Mg-absorption values were previously identified by Jørgensen (1997). In agreement with this trend, we can also argue that our H β' values are slightly higher (i.e., younger) than the cluster sample. This may be one indication that on average our OAGH sample is relatively younger in comparison to the mean age of galaxies in Fornax.

The bottom panels in Figures 9 and 10 show the residuals from the Index'- σ_0 fits ($Y|X$). The dashed lines indicate the 1- σ intrinsic scatter; that is +0.016 and +0.004 mag for Mg b' and $\langle Fe \rangle'$ respectively. We have estimated the intrinsic scatter by requiring

Table 9. Least square fit results.

Index		$\langle \Delta \text{Index}' \rangle$ [mag]	$\langle \delta \text{Index}' \rangle$ [mag]	$\langle \delta i \rangle$ [mag]	R^\dagger
Mg ₂	=	-0.198(±0.048)+0.218(±0.021)· log σ_0	0.024	0.003	0.023
Mgb'	=	-0.277(±0.012)+0.190(±0.005)· log σ_0	0.016	0.004	0.016
$\langle \text{Fe} \rangle'$	=	0.003(±0.014)+0.044(±0.006)· log σ_0	0.007	0.005	0.004
CN ₁	=	-0.457(±0.069)+0.244(±0.030)· log σ_0	0.036	0.006	0.035
H β'	=	0.267(±0.028)-0.086(±0.012)· log σ_0	0.012	0.003	0.011
H γ_A'	=	0.110(±0.033)-0.108(±0.015)· log σ_0	0.016	0.004	0.015

† R is the linear correlation coefficient calculated as $R = \sqrt{bb'}$, where

$\log \sigma_0 = a + b \text{ Index}'$, and $\text{Index}' = a' + b' \log \sigma_0$. The correlation R varies from 0 to 1.

$\langle \Delta \text{Index}' \rangle$: Average deviation from fit (excluding NGC 3156).

$\langle \delta \text{Index}' \rangle$: Average individual error in the index.

$\langle \delta i \rangle$: Estimated intrinsic scatter (excluding NGC 3156).

Table 11. Correlation matrix of the residuals (Δ) of the $\log \sigma_0$ -Index relations.

	ΔMg_2 [mag]	$\Delta \text{Mgb}'$ [mag]	$\Delta \langle \text{Fe} \rangle'$ [mag]	ΔCN_1 [mag]	$\Delta \text{H}\beta'$ [mag]	$\Delta \text{H}\gamma_A'$ [mag]
M_B [mag]	0.17	0.40	0.11	0.17	0.02	0.22
$\log \sigma_0$ [mag]	0.08	0.27	0.19	0.03	0.08	0.36
Mg ₂ [mag]	0.66	0.24	0.48	0.46	0.39	0.66
Mgb' [mag]	0.57	0.38	0.46	0.39	0.42	0.64
$\langle \text{Fe} \rangle'$ [mag]	0.45	0.17	0.84	0.32	0.43	0.78
CN ₁ [mag]	0.59	0.26	0.40	0.71	0.31	0.52
H β' [mag]	0.47	0.21	0.47	0.30	0.82	0.78
H γ_A' [mag]	0.51	0.22	0.67	0.32	0.62	0.94

Note: Linear correlation coefficients (R) calculated as $R = \sqrt{bb'}$, where $\log \sigma_0 = a + b \text{ Index}'$, and $\text{Index}' = a' + b' \log \sigma_0$.

The correlation R varies from 0 to 1.

$$\sum_{k=1}^N \frac{\Delta \text{Index}'_k^2}{\delta \text{Index}'_k^2 + \delta i^2} \equiv 1 \quad (14)$$

where $\Delta \text{Index}'_k$ is the deviation from the fitting relation for each galaxy, $\delta \text{Index}'_k$ are the individual errors in Index' , and δi is the estimated intrinsic scatter. The values for the intrinsic scatter are shown in the last column of Table 9. Comparing with previous results, Colless *et al.* (1999) analysed 736 early-type galaxies from their EFAR cluster galaxy sample with an intrinsic scatter for Mgb' of 0.016 mag. Kuntschner *et al.* (2001), for a sample of 72 early-type galaxies from different environmental regions, derived an intrinsic scatter of 0.012 mag in Mgb', smaller than ours by 0.004 mag.

In Figure 9-a, the Mg₂- σ_0 relation, we also show the least square bisector fit by Guzmán *et al.* (1992) from a sample of 51 Coma cluster ellipticals. The Coma cluster is the densest cluster in the local universe (at average distance ~ 7000 km/s). The bisector fit by Guzmán *et al.* (1992) is

$$\text{Mg}_2 = -(0.316 \pm 0.003) + 0.260 \log \sigma_0 \quad (15)$$

The observed scatter for their Mg₂- σ relation is 0.020 mag. The intrinsic scatter is 0.016 ± 0.002 mag. Guzmán *et al.*'s fit is very similar to the results of Colless *et al.* (1999) for the EFAR sample of cluster galaxies. Colless *et al.* (1999) maximum likelihood fit for Mg₂- σ relation of 423 cluster early-type galaxies is $\text{Mg}_2 = -(0.305 \pm 0.064) + (0.257 \pm 0.027) \log \sigma_0$.

Note that the slope of our fit for the Mg₂- σ_0 relation is

similar to the slopes of the EFAR and Coma cluster samples. However, comparing only the slopes and scatter of the relations is not telling us about important differences between the samples: we would need to analyse the distribution of the galaxies in the Mg- σ relations to infer further conclusions about the different environment (cluster, field). Indeed, most of the galaxies in the EFAR sample are clustered around $\log \sigma \sim 2.35$ -2.40, and go beyond $\log \sigma = 2.5$, which is a slightly different range of σ values from that covered by our group, field and isolated galaxies. We can do a better comparison with the Coma cluster sample of Guzmán *et al.* (1992) as they list the velocity dispersions and Mg₂ index strength for their sample. The average $\log \sigma_0$ in Guzmán *et al.*'s sample is 2.32 (error of the mean: 0.02, for a sample of 51 galaxies), whereas in our sample the average value is $\log \sigma_0 = 2.302$ (error of the mean: 0.014, for a sample of 86 galaxies). The average Mg₂ index strength in the Coma cluster sample is 0.282 (error of the mean: 0.004) and in our sample is 0.307 (error of the mean: 0.004). Thus, the distribution of galaxies in the Mg₂- σ_0 relation for high or less dense regions is very similar. We learn from these comparisons that, perhaps surprisingly, cluster, group and field galaxies have very similar Mg- σ relations, and environment does not seem to be a key parameter here. It is relevant to note here that Bernardi *et al.* (1998) also found, for a large sample of 931 early-type galaxies, that objects assigned to cluster, group or field follow almost identical Mg₂- σ_0 relations.

We note that age and metallicity may conspire to keep

the relation tight (Trager et al. 2000b) and hence its usefulness as a probe of different galactic environments may be limited.

What causes the spread in the Index'- σ_0 relations?

Two obvious potential sources of scatter are age and metallicity. In the case of the Mg- σ_0 relation, it has been investigated by many authors, but perhaps the best paper on this topic is by Bender *et al.* (1993). They conclude that if the spread in the Mg- σ_0 relation at a given σ_0 is due to age only then the rms spread in age is only 15% for bright dynamically hot galaxies. Alternatively, if the spread is only due to metallicity then they infer a rms spread of about 15% in metallicity. A similar analysis by Colless *et al.* (1999) using up-to-date model predictions and constraints from the Fundamental Plane find slightly larger numbers.

With the help of stellar population models one can translate the intrinsic spread in Mgb' for example, at a given σ , into age and metallicity spreads. To simplify this exercise, we assume initially that there are no other sources of scatter, and that age and metallicity are not correlated, or only mildly so (see Colless *et al.* 1999 for more detailed analysis). Using Colless *et al.* (1999) calibration of Mgb' as a function of log age and metallicity, we find for our data set at a given σ and at fixed metallicity a spread of $\delta t/t = 67$ per cent in age and at fixed age a spread of $\delta Z/Z = 43$ per cent respectively. Kuntschner *et al.* (2001) found 49 and 32 per cent respectively.

In Table 11 we investigate the effects that age (in the form of the Balmer-line indices, H β , H γ , for example), metallicity (using Mg, Fe, as metallicity indicators), absolute magnitude (M_B), and σ_0 may have on the scatter of the Index- σ_0 relations. Table 11 presents the results of the linear correlations coefficients (R) from the residuals (Δ) *vs* M_B , $\log \sigma_0$, Mg, Fe, H β , H γ and CN indices.

In general the residuals of the Index- σ_0 relations better correlate with the strength of the Index itself, i.e., ΔMg_2 shows $R = 0.66$ for a correlation with Mg_2 , $\Delta H\beta'$ shows $R = 0.82$ for a correlation with $H\beta'$, and so on. For the Mg_2 - σ_0 , the scatter of the relation grows with decreasing Mg_2 strength. In the case of $H\beta'$ - σ_0 , the scatter grows with increasing $H\beta$ strength. Note however that our sample, like most of the currently available samples, is not complete and is still lacking low-luminosity and low- σ galaxies. Another work by Concannon, Rose & Caldwell (2000) indicates that the spread in age at a given σ increases towards the low velocity dispersion range. Hence incompleteness at low velocity dispersions is potentially a source for bias. Finally, the correlation of the residuals with $H\beta$ index is not specially significant to clearly associate the intrinsic scatters in our sample with possible age variations. The same weak correlations are observed for metal-line indices *vs* scatter, for our sample.

There may well be other effects responsible for the scatter, such as variations in the Mg-overabundance at a given σ_0 . We leave further discussion to a forthcoming paper where we investigate the relations of σ_0 with age, metallicity and α/Fe ratios and the scatter of the Mg- σ_0 relation with age and metallicity.

Finally, we would like to comment on the work of Worthey and Collobert (2003), using a compilation of nearly 2000 Mg- σ relations from the literature to assess the ques-

tion of the importance of mergers in the formation of early-type galaxies. Their simulations suggest that the evolution of median Mg index strength is not a good discriminator between mergers and passive evolution and that better discriminator such as Mg- σ scatter and asymmetry require samples of more than 1000 objects with accuracies similar to today's local measurements to really establish further constraints in the formation scenario of early-type galaxies.

8 SUMMARY

We have argued that there is a sparsity of field and group galaxies in stellar population studies. Many predictions of the hierarchical clustering models compare the properties of field, cluster and group galaxies, however most of the field and group galaxy data available to date tend to be of lower quality than the cluster data. We hope that this work and its high quality data will serve as a step to improve the present state of knowledge based on early-type galaxies from low-density environments.

We carried out an observationally homogeneous survey of 86 local early-type galaxies of mainly group (65), field (10) and isolated (8) objects with the aim of determining nuclear parameters, kinematic (this paper), age and metallicity gradients (subsequent paper).

It is important to emphasize that our survey has the advantage of covering a large wavelength range, from ~ 3850 Å to 6700 Å, giving H α information which is important for emission correction (Section 4.2).

Most of the galaxies in the sample do not show obvious signs of disturbances nor tidal features in their morphologies, although 11 galaxies belong to the Arp catalogue of peculiar galaxies (Arp 1966), of which only three (NGC 750, NGC 751 and NGC 3226) seem to be strongly interacting. Of the 86 galaxies with $S/N \geq 15$ (per resolution element, for $r_e/8$ aperture), 57 had $H\beta$ -index corrected for emission, the average correction was $+0.190$ Å in $H\beta$; 42 galaxies have [O III] $\lambda 5007$ emission correction, of which only 16 also show H α emission.

Our data allowed us to apply a better method for emission correction of the Balmer-line indices than the use of the uncertain $0.6 \times [O\text{ III}]$ estimation. The new correction uses the intensity and equivalent width of the H α index (defined in Table 6). We note that nebular emission could still be affecting the ages and metallicities derived from most of the data in the literature.

A central aspect of this work is that the determination of the errors in all of the measured and derived parameters is based on the analysis of the distribution of repeated observations. In this paper we are presenting data which have the advantage of several repeated observations (measurements) per galaxy. On average, to each galaxy we have eight corresponding spectral frames.

Our main findings are that the index- σ_0 relations presented for low-density regions are not significantly different from those of cluster E/S0s. The slope of the index- σ_0 relations shown in Section 7 does not seem to change for early-type galaxies of different environmental densities, but the scatter of the relations seems larger for group, field and isolated galaxies than for cluster galaxies.

A thorough analysis of the highest signal-to-noise galax-

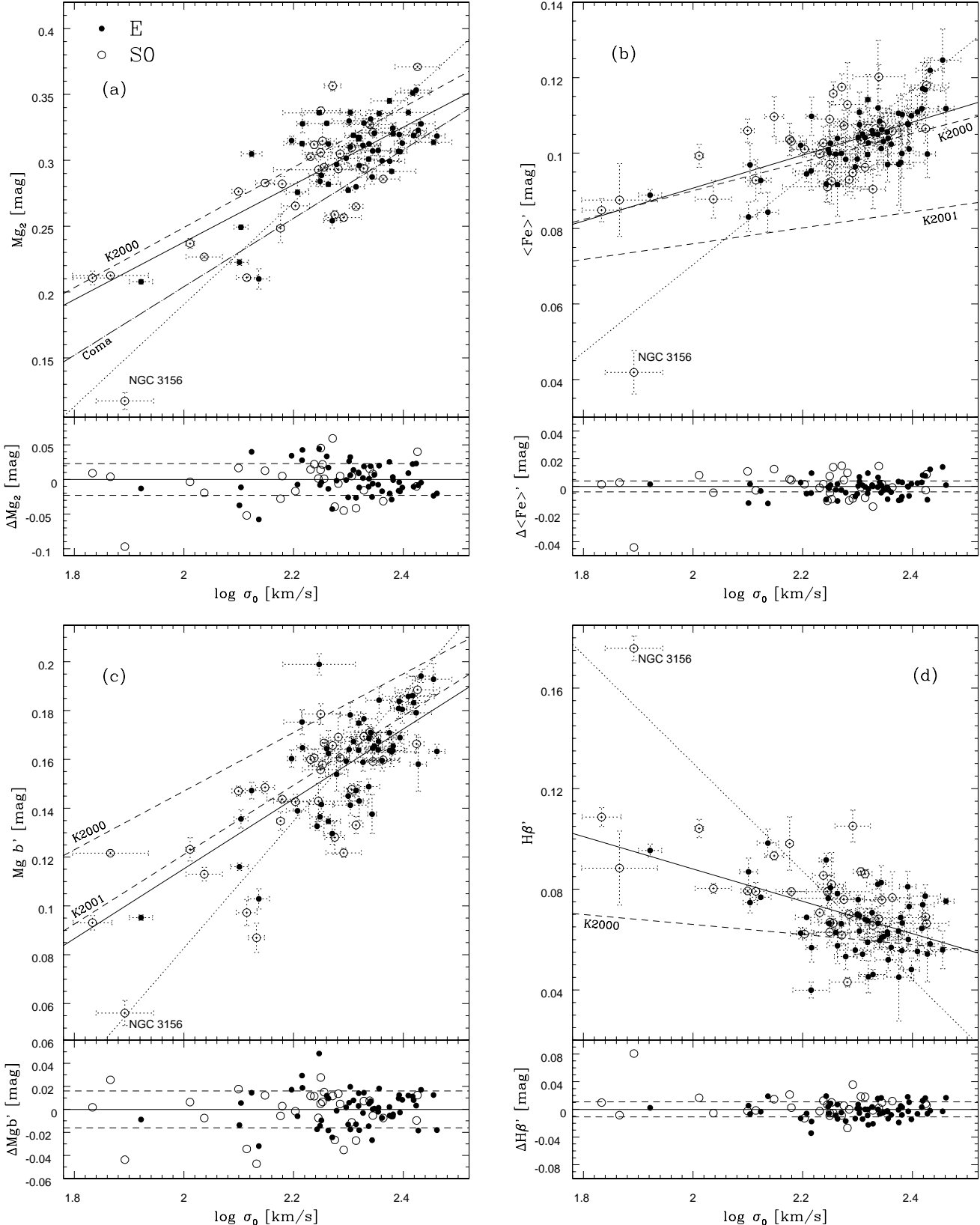


Figure 9. (a) Mg_2 vs $\log \sigma_0$; (b) $\langle Fe \rangle'$ vs $\log \sigma_0$; (c) $Mg b'$ vs $\log \sigma_0$; (d) $H\beta'$ vs $\log \sigma_0$ relations. The indices are measured in magnitudes. The dashed line indicates the fit for the cluster sample of Kuntschner (2000, K2000) and the cluster+field sample of Kuntschner *et al.* (2001, K2001). The dot-dashed line in panel (a) represents the least square bisector fit by Guzmán *et al.* (1992) using a sample of 51 Coma cluster ellipticals. Two fits are shown for our galaxy sample: the solid line is a normal least square fit with the index as dependent variable, and the dotted line is the ordinary least square fit with $\log \sigma_0$ as dependent variable. The residuals of the relations, shown in the lower panels, are calculated with respect to the solid line fits. The dashed lines in the bottom panels indicate the $1-\sigma$ intrinsic scatter in the residuals.

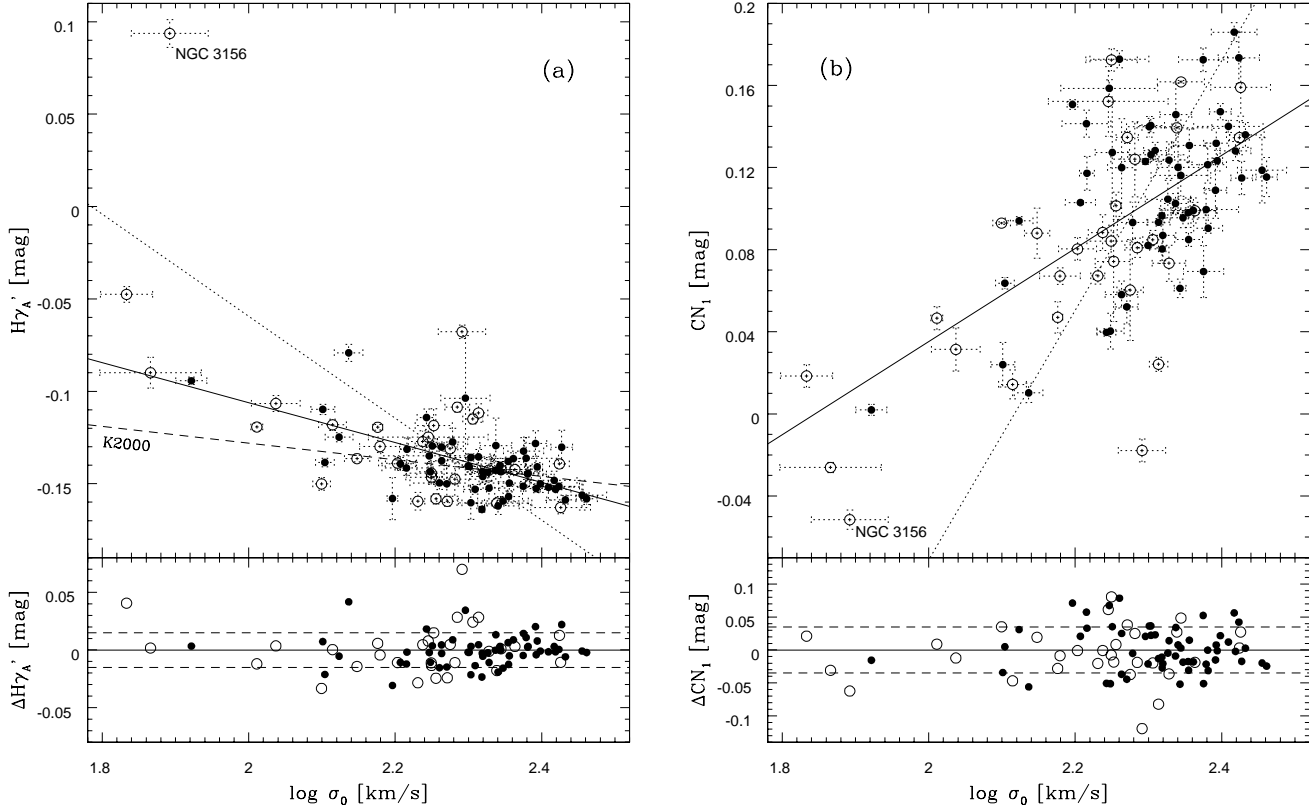


Figure 10. (a) $H\gamma_A'$ vs $\log \sigma_0$; (b) CN_1 vs $\log \sigma_0$ relations. The indices are measured in magnitudes. The dashed line indicates the fit for the cluster sample of Kuntschner (2000, K2000). Two fits are shown for our galaxy sample: the solid line is a normal least square fit with the index as dependent variable, and the dotted line is the ordinary least square fit with $\log \sigma_0$ as dependent variable. The residuals of the relations, shown in the lower panels, are calculated with respect to the solid line fits. The dashed lines in the bottom panels indicate the $1-\sigma$ intrinsic scatter in the residuals.

ies with discussions on the age and metallicity determinations is presented in a forthcoming paper.

ACKNOWLEDGEMENTS

GD would like to thank CNPq-Brazil for the PhD fellowship, INAOE for hospitality during the visits to Mexico, Selwyn College and Cambridge Philosophical Society for financial support. The authors are grateful to the INAOE Committee for telescope time for supporting this project for five consecutive semesters and to the staff at Cananea for cheerful logistic help during the observations. We thank Amâncio Friaça and Alessandro Bressan for several interesting discussions, Max Pettini and Alfonso Aragón-Salamanca for substantial comments to improve this work, and Ewan O'Sullivan for providing us with the details of the isolated sample selection previous to publication. We also thank an anonymous referee for a very thorough analysis of the manuscript. RJT and ET acknowledge the Mexican Research Council Project grants 40018-A-1 and E32186, respectively.

REFERENCES

- Arp H.C., 1966, ApJS, 14, 1
- Baugh C.M., Cole S., Frenk C.S. & Lacey C.G., 1998, ApJ, 498, 504
- Bender R., Burstein D., Faber S.M., 1993, ApJ, 411, 153
- Bender R., Saglia R.P., Gerhard O.E., 1994, MNRAS, 269, 785
- Berlind A.A., Weinberg D.H., Benson A.J., Baugh C.M., Cole S., Davé R., Frenk C.S., Jenkins A., Katz N. & Lacey C.G., 2003, ApJ, 593, 1
- Bernardi M., Renzini, A., da Costa L.N., Wegner G., Alonso M.V., Pellegrini P.S., Ritè C., Willmer C.N.A., 1998, ApJ, 508, L43
- Bevington P.R., 1969, *Data Reduction and Error Analysis for the Physical Sciences*, McGraw-Hill
- Binette L., Magris C.G., Stasińska G., Bruzual A.G., 1994, A&A, 292, 13
- Bower R.G., Lucey J.R. & Ellis R.S., 1992, MNRAS, 254, 601
- Bower R.G., Terlevich A., Kodama T., Caldwell N., 1998, astro-ph/9808325
- Burstein D., Faber S.M., Gaskell C.M., Krumm N., 1984, ApJ, 287, 586
- Burstein D., Bertola F., Buson L.M., Faber S.M., Lauer T.R., 1988, ApJ, 328, 440
- Buzzoni A., Mantegazza L., Gariboldi G., 1994, AJ, 107, 513
- Caldwell N., 1984, PASP, 96, 287
- Cardiel N., Gorgas J., Cenarro J., González J.J., 1998, A&AS, 127, 597
- Carrasco L., Buzzoni A., Salsa M., Recillas-Cruz E., 1996, ASP Conf. Ser. 86, 235
- Cen R. & Ostriker J.P., 1992, ApJ, 399, L113
- Chiosi C. & Carraro G., 2002, MNRAS, 335, 335
- Colbert J.W., Mulchaey J.S., Zabludoff A.I., 2001, AJ, 121, 808
- Colina L. & Arribas S., 1999, ApJ, 514, 637

- Colless M., Burstein D., Davies R.L., McMahan R.K., Saglia R.P., Wegner G., 1999, MNRAS, 303, 813
- Concannon K.D., Rose J.A., Caldwell N., 2000, ApJ, 536, 19
- Covino S., Galletti S., Pasinetti L.E., 1995, A&A, 303, 79
- Davies R.L., Burstein D., Dressler A., Faber S.M., Lynden-Bell D., Terlevich R.J., Wegner G., 1987, ApJS, 64, 581
- de Freitas Pacheco J.A. & Barbuy B., 1995, A&A, 302, 718
- Dressler A., 1984, ApJ, 286, 97
- Faber S.M., Friel E.D., Burstein D., Gaskell C.M., 1985, ApJS, 57, 711
- Filippenko A. & Terlevich R., 1992, ApJ, 397, 79
- Forbes D.A., 1991, MNRAS, 249, 779
- Franx M., Illingworth G., Heckman T., 1989, ApJ, 344, 613
- Garcia A.M., 1993, A&AS, 100, 47
- González J.J., 1993, PhD thesis, Univ. California
- Gregg M.D., 1994, AJ, 108, 2164
- Guzmán R., Lucey J.R., Carter D., Terlevich R.J., 1992, MNRAS, 257, 187
- Isobe T., Feigelson E.D., Akritas M.G., Babu G.J., 1990, ApJ, 364, 104
- Jones L.A. & Worthey G., 1995, ApJ, 446, L31
- Jørgensen I., Franx M. & Kajærgaard P., 1995, MNRAS, 276, 1341
- Jørgensen I., 1997, MNRAS, 288, 161
- Kauffmann G. & Charlot S., 1998, MNRAS, 297, 23
- Kauffmann G., Colberg J.M., Diaferio A. & White S.D.M., 1999, MNRAS, 303, 188
- Kauffmann G., White S.D.M., Heckman T.M., Ménard B., Brinchmann J., Charlot S., Tremonti C., & Brinkmann J., 2004, MNRAS, 353, 713
- Kay S.T., Pearce F.R., Frenk C.S. & Jenkins A., 2002, MNRAS, 330, 113
- Kuntschner H., 1998, PhD thesis, Univ. of Durham
- Kuntschner H. & Davies R.L., 1998, MNRAS, 295, 29
- Kuntschner H., 2000, MNRAS, 315, 184
- Kuntschner H., Lucey J.R., Smith R.J., Hudson M.J. & Davies R.L., 2001, MNRAS, 323, 615
- Kuntschner H., Smith R.J., Colless M., Davies R.L., Kaldare R., Vazdekis, A., 2002, MNRAS, 337, 172
- Maraston C. & Thomas D., 2000, ApJ, 541, 126
- Maraston C., Greggio L., Renzini A., Ortolani S., Saglia R.P., Puzia T.H., Kissler-Patig M., 2003, A&A, 400, 823
- Oke J.B., 1990, AJ, 99, 1621
- Osterbrock D.E., 1989, Astrophysics of Gaseous Nebulae and Active Galactic Nuclei, Mill Valley: University Science Books
- Pearce F.R., Jenkins A., Frenk C.S., Colberg J.M., White S.D.M., Thomas P.A., Couchman H.M.P., Peacock J.A., Efstathiou G. & The Virgo Consortium, 1999, ApJ, 521, L99
- Peterson R.C., Carney B.W., Dorman B., Green E.M., Landsman W., Liebert J., O'Connell R.W., Rood R.T., 2003, ApJ, 588, 299
- Phillips M.M., Jenkins C.R., Dopita M.A., Sadler E.M., Binette L., 1986, AJ, 92, 503
- Prugniel P. & Simien F., 1996, A&A, 309, 749 (PS96)
- Reda F., Forbes D.A., O'Sullivan E., Goudfrooij P., 2004, submitted to MNRAS
- Somerville R.S., & Primack J.R., 1999, MNRAS, 310, 1087
- Terlevich R., Davies R.L., Faber S.M., Burstein D., 1981, MNRAS, 196, 381
- Terlevich A.I. & Forbes D., 2002, MNRAS, 330, 547 (TF02)
- Thomas D., Maraston C. & Bender R., 2003, MNRAS, 339, 897 (TMB03)
- Tonry J. & Davis M., 1981, ApJ, 246, 666
- Trager S.C., 1997, PhD Thesis, Univ. of California, Santa Cruz
- Trager S.C., Worthey G., Faber S.M., Burstein D. & González J.J., 1998, ApJS, 166, 1
- Trager S.C., Faber S.M., Worthey G., González J.J., 2000, AJ, 119, 1645 (2000a)
- Trager S.C., Faber S.M., Worthey G., González J.J., 2000, AJ, 120, 165 (2000b)
- Tran H.D., Tsvetanov Z., Ford H.C., Davies J., Jaffe W., van den Bosch F.C., Rest A., 2001, AJ, 121, 2928
- Tully R.B., 1987, Nearby Galaxy Catalog (Cambridge: Cambridge University Press)
- White S.D.M. & Rees M.J., 1978, MNRAS, 183, 341
- Willis J.P., Hewett P.C., Warren S.J., Lewis G.F., 2002, MNRAS, 337, 953
- Worthey G., Faber S.M., González J.J. & Burstein D., 1994, ApJS, 94, 687
- Worthey G., 1994, ApJS, 95, 107 (W94)
- Worthey G. & Ottaviani D.L., 1997, ApJS, 111, 377
- Worthey G. & Collobert M., 2003, ApJ, 586, 17

APPENDIX A: SAMPLE COMPLEMENTARY INFORMATION

Table A1 contains complementary information about the galaxy sample, including environment information and our classification as group, field and isolated galaxy.

APPENDIX B: FULLY CORRECTED LINE-STRENGTH INDICES

We present the final corrected central $r_e/8$ index measurements and associated errors for our galaxy sample. The Lick indices presented in Table B.1 were calibrated to the Lick/IDS system, and corrected for velocity dispersion and nebular emission (in this case mainly the Balmer lines).

Table A1. Complementary details of the galaxy sample.

Name	Type	V_{rot} (km/s)	r_e (")	$\log R_{25}$	PA_{maj} ($^{\circ}$)	FP_{res}	Environment information
ESO462-G015	-5	-	21	0.11	166	-0.05	Isolated
MCG-01-03-018	-3	-	23*	0.00		0.29	Isolated
NGC 0016	-3	160	28*	0.27	16	0.02	Field
NGC 0221	-6	46	36	0.13	170	0.19	M32, dwarf companion of M31, group (LGG 11)
NGC 0315	-4	32	37	0.20	40	0.09	Group (LGG 14)
NGC 0474	-2	-	34	0.05	75	0.11	Arp227, group (LGG 20)
NGC 0584	-5	157	25	0.26	55	-0.28	Group (LGG 27)
NGC 0720	-5	48	36	0.29	140	0.02	Group (LGG 38)
NGC 0750	-5	40	27*	0.10		0.04	Arp166, pair with NGC 0751, group (LGG 42)
NGC 0751	-5	-	22*	0.00		0.20	Arp166, pair with NGC 0750, group (LGG 42)
NGC 0777	-5	53	34	0.08	155	0.15	Group (LGG 42)
NGC 0821	-5	89	50	0.20	25	0.28	Isolated
NGC 0890	-3	-	34	0.16	50*	-0.17	Field
NGC 1045	-3	-	36*	0.28	40	0.19	Isolated
NGC 1052	-5	101	34	0.16	120	0.32	Group (LGG 71)
NGC 1132	-4.5	-	34	0.27	140	0.06	Isolated
NGC 1407	-5	30	70	0.03	35	0.21	Eridanus group (LGG 100)
NGC 1453	-5	-	25	0.09		0.29	Group (LGG 103)
NGC 1600	-5	4	45	0.17	15	0.20	Field
NGC 1700	-5	75	18	0.20	90	-0.51	Group (LGG 123)
NGC 1726	-2	40	24	0.12	170	-0.10	Field
NGC 2128	-3	-	23*	0.13	60	0.51	Isolated
NGC 2300	-2	6	31	0.14		0.44	Arp114, group (LGG 145)
NGC 2418	-5	142	28*	0.00		0.31	Arp165, field
NGC 2513	-5	53	33	0.09	170	0.19	Field
NGC 2549	-2	115	17	0.48	177	-0.03	Field
NGC 2768	-5	78	64	0.28	95	-0.06	Group (LGG 167)
NGC 2872	-5	75	18	0.06	22	0.17	Arp307, field
NGC 2911	-2	-	51	0.11	140	0.17	Arp232, group (LGG 177)
NGC 2974	-5	202	24	0.23	40	0.21	Group (LGG 179)
NGC 3091	-5	71	33	0.20	149	0.27	Group (LGG 186)
NGC 3098	-2	130	15	0.57	90	-0.12	Field
NGC 3115	-3	273	32	0.47	40	-0.11	Field
NGC 3139	-2	-	22*	0.08		1.46	Field
NGC 3156	-2	79	14	0.24	47	-0.54	Group (LGG 192)
NGC 3193	-5	80	27	0.05		0.26	Arp316, group (LGG 194)
NGC 3226	-5	40	34	0.05	15	0.40	Arp094, group (LGG 194)
NGC 3245	-2	-	27	0.26	177	0.09	Group (LGG 197)
NGC 3377	-5	86	34	0.24	35	0.03	Leo group (LGG 217)
NGC 3379	-5	53	35	0.05		-0.18	Leo group (LGG 217)
NGC 3384	-3	-	25	0.34	53	-0.23	Leo group (LGG 217)
NGC 3412	-2	-	26	0.25	155	-0.38	Leo group (LGG 217)
NGC 3414	-2	63	21	0.14		0.18	Arp162, group (LGG 227)
NGC 3599	-2	-	24	0.10		-0.12	Field
NGC 3607	-2	108	43	0.30	120	0.22	Field
NGC 3608	-5	26	34	0.09	75	0.27	Group (LGG 237)
NGC 3610	-5	143	15	0.07		-0.50	Group (LGG 234)
NGC 3613	-5	141	27	0.32	102	-0.04	Group (LGG 232)
NGC 3636	-5	-	20*	0.00		-0.04	Group (LGG 235)
NGC 3640	-5	114	32	0.10	100	0.00	Group (LGG 233)
NGC 3665	-2	103	29	0.08	30	0.00	Group (LGG 236)
NGC 3923	-5	-	50	0.18	50	0.01	Group (LGG 255)
NGC 3941	-2	-	23	0.18	10	-0.39	Field
NGC 4125	-5	97	58	0.26	95	0.05	Group (LGG 274)
NGC 4261	-5	69	36	0.05	160	0.13	3C270, group (LGG 278)
NGC 4365	-5	43	50	0.14	40	0.04	Virgo, group (LGG 289)
NGC 4374	-5	23	51	0.06	135	0.08	Virgo, group (LGG 292)
NGC 4494	-5	67	49	0.13		-0.33	Group (LGG 294)
NGC 4550	-1.5	122	15	0.55	178	-0.03	Field
NGC 4754	-3	89	26	0.27	23	-0.08	Virgo, group (LGG 289)
NGC 5322	-5	20	34	0.18	95	-0.07	Group (LGG 360)
NGC 5353	-2	-	15	0.30	145	0.03	Group (LGG 363)
NGC 5354	-2	-	18	0.04		-0.14	Group (LGG 361)

Table A1. Continued.

Name	Type	V_{rot} (km/s)	r_e (")	$\log R_{25}$	PA_{maj} ($^{\circ}$)	FP_{res}	Environment information
NGC 5363	90.0	-	36	0.19	135	0.06	Group (LGG 362)
NGC 5444	-4	-	27	0.06	90	0.17	Group (LGG 370)
NGC 5557	-5	-	30	0.09	105	-0.04	Group (LGG 378)
NGC 5576	-5	14	18	0.20	95	-0.14	Group (LGG 379)
NGC 5638	-5	62	28	0.05	150	-0.01	Group (LGG 386)
NGC 5812	-5	40	26	0.06		0.24	Field
NGC 5813	-5	36	57	0.14	145	0.23	Group (LGG 393)
NGC 5831	-5	27	26	0.04	55	0.24	Group (LGG 393)
NGC 5845	-4.6	127	12*	0.19	150	0.81	Group (LGG 392)
NGC 5846	-5	4	62	0.03		0.12	Pair with NGC 5846A, group (LGG 393)
NGC 5846 A	-6	74	6*	0.15	120	0.35	Pair with NGC 5846, group (LGG 393)
NGC 5854	-1	-	15	0.54	55	-0.24	Group (LGG 393)
NGC 5864	-2	-	44*	0.49	68	0.24	Group (LGG 393)
NGC 5869	-2	-	36*	0.14	125	0.32	Group (LGG 393)
NGC 5982	-5	45	24	0.12	110	0.00	Group (LGG 402)
NGC 6172	-4	-	16*	0.00		-0.12	Isolated
NGC 6411	-5	14	29	0.10	70	-0.18	Isolated
NGC 7302	-3	-	13	0.21	100*	0.15	Field
NGC 7332	-2	134	15	0.56	155	-0.30	Field
NGC 7454	-5	23	25	0.15	150	-0.07	Group (LGG 469)
NGC 7585	-1	-	24	0.07	105	-0.09	Arp223, field
NGC 7619	-5	69	37	0.04	30	0.29	Pegasus I group (LGG 473)
NGC 7626	-5	20	39	0.05		0.25	Pegasus I group (LGG 473)

References: Morphologies are from the *Third Reference Catalogue* (RC3). The maximum rotation velocity V_{rot} is from Prugniel & Simien (1996). Effective radius r_e and the R_{25} parameter are from Trager *et al.* (2000b) and RC3 catalog. The Fundamental Plane residual FP_{res} was derived from eq.(4) in Prugniel & Simien (1996). The asterisk symbols assign estimates made by the authors. Environmental information is from E. O'Sullivan (private communication); the group identification was extracted from Garcia 1993 (LGG group number in parenthesis).

Galaxy	H δ_A [Å]	H δ_F [Å]	H γ_A [Å]	H γ_F [Å]	CN ₁ [mag]	CN ₂ [mag]	Ca4227 [Å]	G4300 [Å]	Fe4383 [Å]	Ca4455 [Å]	Fe4531 [Å]	C ₂ 4668 [Å]	H β [Å]	Fe5015 [Å]	Mg ₁ [mag]	Mg ₂ [mag]	Mg _b [Å]	Fe5270 [Å]	Fe5335 [Å]	Fe5406 [Å]	Fe5709 [Å]	Fe5782 [Å]	NaD [Å]	TiO ₁ [mag]	TiO ₂ [mag]
ESO462-G015	-2.40	0.15	-5.85	-1.43	0.100	0.143	1.47	5.44	5.31	1.79	3.58	8.21	1.76	4.66	0.104	0.292	4.53	2.73	3.40	1.87	0.79	1.29	4.77	0.040	0.070
±	0.30	0.43	0.55	0.44	0.011	0.016	0.20	0.21	0.45	0.14	0.18	0.18	0.05	0.25	0.005	0.001	0.16	0.44	0.25	0.35	0.15	0.31	0.28	0.002	0.006
MCG01-03-018	-3.21	-0.57	-6.37	-1.43	0.124	0.165	1.29	5.57	6.53	1.78	4.30	8.23	1.12	5.16	0.112	0.293	4.69	3.34	3.37	1.82	0.95	1.07	5.14	0.065	0.096
±	0.49	0.41	0.52	0.34	0.018	0.021	0.07	0.50	0.61	0.41	0.16	0.57	0.05	0.23	0.004	0.011	0.24	0.18	0.15	0.11	0.09	0.14	0.10	0.005	0.003
NGC 0016	-1.68	0.62	-5.56	-1.23	0.067	0.111	1.16	5.18	5.93	1.64	3.62	8.47	2.02	5.89	0.121	0.282	4.03	3.30	2.92	1.71	0.94	1.25	4.42	0.032	0.074
±	0.24	0.15	0.17	0.03	0.006	0.006	0.07	0.05	0.17	0.07	0.20	0.37	0.02	0.18	0.001	0.006	0.07	0.11	0.06	0.11	0.11	0.07	0.09	0.000	0.001
NGC 0221	-0.90	1.01	-3.97	-0.37	0.002	0.036	1.07	4.76	4.87	1.31	3.18	5.92	2.42	5.81	0.092	0.207	2.73	3.02	2.60	1.56	1.00	0.95	3.25	0.047	0.056
±	0.08	0.02	0.09	0.07	0.003	0.002	0.01	0.09	0.11	0.04	0.05	0.19	0.06	0.18	0.005	0.005	0.05	0.05	0.06	0.05	0.01	0.02	0.09	0.001	0.001
NGC 0315	-2.49	0.27	-5.48	-0.93	0.109	0.152	1.31	5.49	5.93	1.87	4.01	8.37	2.01	4.42	0.141	0.307	4.99	3.46	3.23	1.95	0.93	1.40	5.28	0.045	0.078
±	0.48	0.16	0.34	0.19	0.014	0.014	0.09	0.10	0.23	0.17	0.24	0.40	0.17	0.29	0.008	0.008	0.10	0.14	0.17	0.20	0.03	0.14	0.18	0.002	0.002
NGC 0474	-2.41	0.36	-5.97	-1.38	0.080	0.118	1.32	5.45	5.77	1.64	4.01	6.44	1.71	6.03	0.115	0.266	4.00	3.25	2.89	2.05	0.83	0.95	4.11	0.050	0.101
±	0.17	0.06	0.17	0.10	0.005	0.009	0.11	0.03	0.07	0.10	0.25	0.30	0.10	0.27	0.003	0.008	0.01	0.10	0.09	0.13	0.09	0.15	0.001	0.002	
NGC 0584	-2.38	0.38	-6.04	-1.45	0.082	0.121	1.19	5.51	5.49	1.48	3.73	8.08	1.90	6.43	0.122	0.277	4.06	3.34	2.76	1.75	1.00	1.03	4.06	0.042	0.082
±	0.07	0.14	0.22	0.14	0.002	0.004	0.06	0.10	0.14	0.05	0.09	0.23	0.10	0.05	0.007	0.002	0.09	0.09	0.04	0.03	0.05	0.10	0.002	0.000	
NGC 0720	-3.40	-0.05	-6.40	-1.70	0.186	0.244	1.50	5.28	6.63	1.78	3.74	9.40	1.74	5.81	0.174	0.351	5.12	3.56	2.97	1.77	0.80	1.08	6.10	0.051	0.095
±	0.20	0.12	0.23	0.07	0.005	0.004	0.07	0.27	0.11	0.08	0.22	0.59	0.18	0.44	0.001	0.002	0.18	0.15	0.09	0.07	0.05	0.10	0.07	0.002	0.002
NGC 0750	-2.67	-0.16	-5.45	-1.01	0.093	0.134	1.08	5.59	4.60	1.26	4.19	8.29	1.38	4.58	0.119	0.297	4.30	3.55	3.24	1.77	0.75	1.26	5.14	0.048	0.076
±	0.54	0.17	0.35	0.16	0.010	0.014	0.26	0.21	0.56	0.16	0.12	0.36	0.12	0.23	0.004	0.004	0.17	0.04	0.13	0.07	0.18	0.07	0.09	0.003	0.003
NGC 0751	-1.73	0.00	-6.49	-1.57	0.052	0.090	0.95	6.14	5.81	1.05	4.15	7.48	1.70	3.61	0.096	0.254	3.66	3.42	2.57	2.05	0.79	1.33	3.45	0.037	0.066
±	0.57	0.38	0.50	0.26	0.009	0.014	0.17	0.19	0.39	0.08	0.38	0.37	0.09	0.34	0.002	0.006	0.11	0.18	0.23	0.06	0.04	0.08	0.10	0.002	0.002
NGC 0777	-2.62	-0.11	-5.58	-1.32	0.115	0.168	0.99	4.91	5.12	1.52	4.40	10.33	1.40	4.18	0.154	0.322	4.40	3.50	3.03	1.72	0.92	1.18	5.98	0.063	0.110
±	0.51	0.14	0.45	0.24	0.010	0.014	0.17	0.28	0.15	0.05	0.19	0.20	0.26	0.11	0.002	0.008	0.27	0.16	0.24	0.17	0.10	0.09	0.11	0.002	0.003
NGC 0821	-2.76	0.18	-6.20	-1.50	0.104	0.149	1.31	5.36	6.22	1.59	3.75	8.34	1.81	5.44	0.149	0.311	4.42	3.15	3.12	1.75	0.79	1.00	4.46	0.054	0.100
±	0.33	0.17	0.23	0.15	0.009	0.007	0.11	0.24	0.17	0.05	0.15	0.41	0.14	0.07	0.007	0.005	0.09	0.09	0.10	0.09	0.11	0.02	0.03	0.001	0.000
NGC 0890	-1.01	0.74	-4.74	-0.93	0.024	0.058	0.77	4.65	4.97	1.42	4.13	8.50	2.19	6.36	0.104	0.265	3.75	3.32	2.97	1.88	1.06	4.48	4.24	0.045	0.096
±	0.15	0.12	0.24	0.12	0.004	0.007	0.34	0.10	0.30	0.13	0.12	0.47	0.04	0.81	0.001	0.001	0.09	0.16	0.06	0.17	0.08	0.05	0.03	0.002	0.001
NGC 1045	-2.71	0.26	-6.12	-1.57	0.099	0.149	1.44	5.35	5.56	1.58	3.99	8.01	1.94	5.58	0.117	0.286	4.45	3.56	3.24	1.94	0.94	0.98	5.07	0.059	0.104
±	0.10	0.13	0.13	0.14	0.005	0.003	0.09	0.10	0.14	0.09	0.12	0.17	0.26	0.33	0.003	0.002	0.08	0.06	0.14	0.09	0.04	0.06	0.05	0.001	0.004
NGC 1052	-0.45	1.64	-5.72	-0.62	0.158	0.205	1.12	5.77	6.25	1.59	3.60	7.37	1.85	2.50	0.182	0.336	5.44	2.85	2.89	1.83	0.88	1.03	6.28	0.062	0.112
±	0.58	0.50	0.57	0.48	0.005	0.009	0.13	0.29	0.11	0.07	0.12	0.11	0.41	0.09	0.001	0.002	0.12	0.06	0.04	0.04	0.02	0.05	0.06	0.001	0.001
NGC 1132	-2.05	0.51	-5.68	-1.19	0.070	0.109	0.91	5.22	6.07	1.55	3.19	6.53	1.16	3.56	0.133	0.299	4.55	2.63	2.84	1.62	0.83	1.01	4.12	0.044	0.065
±	0.67	0.55	0.37	0.22	0.014	0.008	0.27	0.05	0.63	0.24	0.25	0.64	0.42	0.37	0.004	0.008	0.12	0.09	0.16	0.14	0.06	0.08	0.10	0.003	0.002
NGC 1407	-2.92	-0.18	-6.55	-1.88	0.173	0.232	1.71	5.65	6.64	1.79	3.51	8.78	1.96	5.89	0.178	0.353	4.94	3.65	3.37	1.78	0.83	1.23	5.73	0.068	0.110
±	0.50	0.25	0.09	0.14	0.013	0.012	0.14	0.10	0.27	0.15	0.35	0.33	0.13	0.26	0.005	0.004	0.09	0.14	0.18	0.13	0.08	0.06	0.05	0.002	0.003
NGC 1453	-3.51	0.17	-6.48	-1.73	0.148	0.204	1.43	5.52	5.76	1.88	4.01	9.43	1.21	4.44	0.138	0.313	4.98	3.72	3.32	1.94	0.98	0.95	5.70	0.052	0.121
±	0.29	0.25	0.26	0.11	0.009	0.007	0.17	0.29	0.25	0.14	0.12	0.54	0.13	0.15	0.005	0.003	0.17	0.28	0.12	0.14	0.04	0.08	0.15	0.002	0.003
NGC 1600	-3.33	0.11	-6.62	-1.73	0.128	0.189	1.53	5.65	6.65	1.84	4.12	9.95	1.87	5.87	0.142	0.319	5.05	3.51	3.54	2.18	0.82	1.61	6.15	0.055	0.063
±	0.13	0.33	0.09	0.14	0.008	0.010	0.16	0.11	0.19	0.07	0.19	0.21	0.13	0.24	0.004	0.001	0.10	0.15	0.27	0.06	0.19	0.16	0.31	0.001	0.001
NGC 1700	-1.38	0.66	-6.03	-1.25	0.062	0.101	0.78	5.71	6.03	1.39	3.72	8.72	2.10	5.52	0.122	0.288	3.87	3.16	2.79	1.79	0.98	0.85	4.89	0.051	0.092
±	0.34	0.29	0.06	0.10	0.006	0.003	0.03	0.18	0.17	0.09	0.35	0.09	0.18	0.38	0.002	0.005	0.21	0.08	0.08	0.05	0.01	0.03	0.05	0.003	0.006
NGC 1726	-2.34	0.27	-6.14	-1.67	0.074	0.124	1.27	5.17	4.91	1.60	3.58	8.24	1.67	5.06	0.126	0.294	4.70	3.00	2.75	1.69	0.91	0.80	4.39	0.051	0.106
±	0.33	0.27	0.28	0.07	0.010	0.011	0.12	0.29	0.22	0.19	0.06	0.24	0.18	0.22	0.002	0.003	0.09	0.17	0.12	0.11	0.08	0.05	0.08	0.002	0.005
NGC 2128	-0.69	1.17	-5.03	-0.66	0.075	0.116	1.41	5.13																	

Table B1. Fully corrected Lick/IDS indices for the central re/8 extraction; continued.

Galaxy	H δ_A [Å]	H δ_F [Å]	H γ_A [Å]	H γ_F [Å]	CN ₁ [mag]	CN ₂ [mag]	Ca4227 [Å]	G4300 [Å]	Fe4383 [Å]	Ca4455 [Å]	Fe4531 [Å]	C ₂ 4668 [Å]	H β [Å]	Fe5015 [Å]	Mg ₁ [mag]	Mg ₂ [mag]	Mg _b [Å]	Fe5270 [Å]	Fe5335 [Å]	Fe5406 [Å]	Fe5709 [Å]	Fe5782 [Å]	NaD [Å]	TiO ₁ [mag]	TiO ₂ [mag]	
NGC 2513	-3.13	0.81	-6.61	-1.85	0.132	0.179	1.23	5.49	6.11	1.90	3.86	9.23	1.63	5.30	0.150	0.319	5.06	3.63	2.89	1.99	1.10	0.92	5.53	0.034	0.091	
±	0.37	0.20	0.11	0.06	0.008	0.007	0.09	0.14	0.17	0.12	0.15	0.18	0.11	0.22	0.002	0.004	0.09	0.10	0.17	0.09	0.11	0.10	0.12	0.004	0.003	
NGC 2549	-2.29	0.67	-5.86	-1.02	0.088	0.124	1.33	5.25	6.36	1.60	3.79	9.07	2.36	5.93	0.125	0.283	4.16	3.52	3.02	1.91	0.97	1.07	4.31	0.044	0.108	
±	0.29	0.04	0.08	0.05	0.012	0.011	0.09	0.16	0.31	0.05	0.10	0.63	0.13	0.18	0.001	0.003	0.07	0.08	0.11	0.05	0.19	0.04	0.07	0.001	0.004	
NGC 2768 0°	-2.17	0.47	-6.21	-1.50	0.084	0.122	1.20	5.34	6.37	1.64	3.61	7.22	1.61	4.83	0.146	0.306	4.34	3.44	3.02	1.50	0.96	0.90	3.83	0.031	0.081	
±	0.16	0.17	0.31	0.25	0.008	0.014	0.13	0.11	0.14	0.18	0.13	0.15	0.12	0.12	0.002	0.003	0.08	0.11	0.18	0.09	0.21	0.13	0.13	0.001	0.003	
NGC 2768 90°	-2.40	0.38	-6.85	-1.75	0.102	0.143	1.30	5.54	6.75	1.79	4.11	7.33	1.69	5.45	0.123	0.295	4.63	3.66	3.18	2.02	—	—	—	—	—	—
±	0.14	0.12	0.14	0.13	0.007	0.008	0.09	0.11	0.13	0.01	0.07	0.34	0.07	0.13	0.003	0.002	0.01	0.05	0.09	0.09	—	—	—	—	—	—
NGC 2872	-2.18	0.60	-6.24	-1.79	0.121	0.175	1.38	5.22	5.32	1.76	4.32	8.16	1.54	5.44	0.158	0.325	4.55	3.26	3.13	1.54	1.00	1.20	5.18	0.028	0.086	
±	0.23	0.29	0.21	0.08	0.010	0.011	0.21	0.12	0.32	0.13	0.19	0.30	0.20	0.17	0.003	0.004	0.09	0.15	0.12	0.11	0.10	0.13	0.14	0.002	0.004	
NGC 2911	0.64	2.15	-5.40	-0.64	0.088	0.126	1.24	4.61	6.50	1.38	3.11	6.91	2.12	4.68	0.170	0.312	4.47	2.84	2.87	1.75	0.94	0.89	6.25	0.047	0.091	
±	0.52	0.37	0.40	0.31	0.010	0.012	0.15	0.13	0.27	0.30	0.29	0.61	0.26	0.20	0.003	0.002	0.10	0.10	0.09	0.11	0.07	0.07	0.07	0.003	0.002	
NGC 2974	-2.64	0.56	-4.42	-0.71	0.123	0.166	1.18	5.26	5.44	1.46	3.44	7.92	1.41	4.43	0.143	0.301	4.43	3.10	2.83	2.04	1.00	0.99	4.80	0.036	0.095	
±	0.12	0.15	1.53	0.79	0.002	0.003	0.09	0.04	0.32	0.01	0.10	0.24	0.10	0.10	0.001	0.004	0.09	0.08	0.10	0.06	0.12	0.05	0.05	0.003	0.004	
NGC 3091	-2.69	0.17	-6.77	-1.79	0.119	0.175	1.85	5.26	6.44	1.69	4.43	9.60	1.43	6.34	0.146	0.314	5.29	3.89	4.09	2.01	0.96	1.18	5.52	0.028	0.108	
±	0.37	0.13	0.39	0.20	0.017	0.014	0.30	0.29	0.22	0.18	0.26	0.23	0.19	0.27	0.003	0.002	0.15	0.25	0.22	0.19	0.08	0.31	0.14	0.005	0.002	
NGC 3098	-0.46	0.79	-4.51	-0.79	0.032	0.081	1.16	4.50	4.74	1.43	3.90	5.52	2.05	5.09	0.096	0.227	3.21	3.16	2.44	1.75	1.05	0.94	2.49	0.050	0.069	
±	0.32	0.22	0.19	0.20	0.011	0.013	0.09	0.15	0.23	0.16	0.08	0.19	0.12	0.17	0.002	0.001	0.08	0.18	0.10	0.11	0.03	0.00	0.06	0.002	0.000	
NGC 3115	-3.17	0.01	-6.97	-1.74	0.139	0.187	1.65	5.27	7.01	1.97	3.97	8.45	1.85	6.70	0.158	0.327	4.74	3.62	3.44	1.73	0.94	1.03	5.14	0.050	0.108	
±	0.24	0.18	0.12	0.06	0.001	0.001	0.04	0.17	0.16	0.09	0.04	0.11	0.09	0.10	0.003	0.003	0.06	0.06	0.08	0.05	0.04	0.12	0.001	0.001		
NGC 3139	—	—	—	—	—	—	—	—	—	—	—	—	—	—	—	—	—	—	—	—	—	—	—	—	—	
±	—	—	—	—	—	—	—	—	—	—	—	—	—	—	—	—	—	—	—	—	—	—	—	—	—	
NGC 3156	5.13	4.38	3.61	3.68	-0.051	-0.008	0.44	1.54	1.28	0.54	2.62	2.13	4.29	3.58	0.040	0.117	1.64	1.90	1.63	1.14	0.57	0.38	1.72	0.022	0.024	
±	0.21	0.15	0.28	0.16	0.005	0.003	0.15	0.21	0.15	0.10	0.30	0.31	0.14	0.32	0.004	0.006	0.15	0.30	0.10	0.08	0.08	0.12	0.16	0.004	0.003	
NGC 3193	-2.55	0.09	-6.18	-1.58	0.116	0.164	1.36	5.22	5.91	1.71	4.09	8.25	1.66	5.36	0.139	0.307	4.57	3.47	3.09	1.91	1.05	1.09	4.66	0.049	0.097	
±	0.11	0.06	0.26	0.14	0.010	0.014	0.06	0.12	0.18	0.09	0.21	0.12	0.10	0.05	0.001	0.003	0.12	0.07	0.04	0.10	0.03	0.02	0.05	0.001	0.001	
NGC 3226	-1.34	0.88	-6.07	-1.47	0.142	0.178	1.14	4.66	6.04	1.28	3.72	7.20	1.01	4.02	0.153	0.313	4.85	2.87	2.46	1.68	1.07	1.10	4.93	0.037	0.086	
±	0.39	0.31	0.23	0.14	0.007	0.005	0.05	0.21	0.23	0.08	0.06	0.14	0.13	0.13	0.002	0.002	0.13	0.14	0.12	0.08	0.12	0.08	0.13	0.002	0.002	
NGC 3245	-1.03	0.94	-4.59	-0.57	0.081	0.122	1.04	4.74	5.53	1.60	3.39	8.03	1.77	5.22	0.158	0.305	4.47	2.95	2.55	1.71	0.97	0.88	4.36	0.029	0.092	
±	0.15	0.11	0.16	0.11	0.006	0.005	0.06	0.13	0.08	0.12	0.21	0.09	0.09	0.002	0.006	0.16	0.04	0.14	0.05	0.12	0.09	0.16	0.003	0.002		
NGC 3377	-1.76	0.58	-5.33	-1.05	0.094	0.138	1.00	5.07	5.43	1.29	3.35	7.39	1.96	5.26	0.150	0.305	4.12	2.97	2.60	1.75	0.90	0.89	4.13	0.031	0.084	
±	0.06	0.06	0.12	0.07	0.003	0.002	0.03	0.11	0.16	0.08	0.10	0.13	0.01	0.07	0.002	0.002	0.09	0.03	0.14	0.12	0.05	0.05	0.07	0.002	0.001	
NGC 3379 90°	-2.95	0.04	-6.63	-1.73	0.129	0.178	1.34	5.42	6.18	1.80	3.88	7.95	1.50	6.41	0.162	0.319	4.64	3.13	3.09	1.91	0.95	1.03	5.05	0.052	0.102	
±	0.08	0.04	0.13	0.08	0.005	0.005	0.05	0.06	0.12	0.07	0.07	0.06	0.10	0.16	0.003	0.002	0.05	0.05	0.04	0.03	0.03	0.06	0.002	0.001		
NGC 3379 70°	-2.64	0.13	-7.13	-2.03	0.097	0.138	1.40	5.63	6.50	1.60	3.80	8.64	1.51	5.81	0.162	0.317	4.55	2.97	2.42	1.89	1.00	1.13	4.76	0.049	0.088	
±	0.08	0.19	0.07	0.02	0.004	0.004	0.05	0.08	0.10	0.02	0.06	0.17	0.12	0.08	0.001	0.001	0.08	0.07	0.02	0.10	0.05	0.02	0.04	0.001	0.003	
NGC 3384	-2.39	0.56	-6.92	-1.82	0.067	0.101	1.26	5.56	6.57	1.50	3.71	9.60	1.81	6.63	0.149	0.302	4.45	2.08	3.27	1.91	1.12	1.13	5.08	0.044	0.085	
±	0.08	0.07	0.23	0.09	0.004	0.005	0.03	0.16	0.16	0.10	0.06	0.17	0.07	0.13	0.002	0.002	0.07	0.05	0.05	0.02	0.05	0.06	0.003	0.004		
NGC 3412	-1.64	0.76	-5.08	-0.78	0.047	0.090	1.32	4.99	5.76	1.42	3.55	6.41	2.63	6.58	0.097	0.237	3.48	3.05	2.91	1.71	0.95	0.80	2.93	0.039	0.090	
±	0.12	0.05	0.10	0.07	0.006	0.006	0.10	0.12	0.17	0.11	0.12	0.02	0.09	0.54	0.002	0.004	0.13	0.08	0.07	0.03	0.05	0.04	0.03	0.003	0.001	
NGC 3414	-1.74	0.31	-6.30	-1.43	0.173	0.236	1.43	5.58	5.79	1.60	3.95	8.56	1.68	4.91	0.184	0.337	4.93	3.08	2.64	1.67	0.96	1.01	5.32	0.046	0.091	
±	0.20	0.16	0.19	0.13	0.005	0.007	0.08	0.17	0.12	0.15	0.08	0.23	0.12	0.25	0.003	0.003	0.10	0.07	0.06	0.08	0.04	0.11	0.02	0.001	0.003	
NGC 3599	0.88	1.75	-1.96	0.78	0.018	0.062	0.80	3.36	4.44	1.36	3.27	5.98	2.74	5.10	0.094	0.211	2.67	2.94	2.61	1.46	0.99	0.78	3.02	0.		

Galaxy	$H\delta_A$ [Å]	$H\delta_F$ [Å]	$H\gamma_A$ [Å]	$H\gamma_F$ [Å]	CN ₁ [mag]	CN ₂ [mag]	Ca4227 [Å]	G4300 [Å]	Fe4383 [Å]	Ca4455 [Å]	Fe4531 [Å]	C ₂ 4668 [Å]	H β [Å]	Fe5015 [Å]	Mg ₁ [mag]	Mg ₂ [mag]	Mg _b [Å]	Fe5270 [Å]	Fe5335 [Å]	Fe5406 [Å]	Fe5709 [Å]	Fe5782 [Å]	NaD [Å]	TiO ₁ [mag]	TiO ₂ [mag]	
NGC 3613	-2.53	0.35	-5.82	-1.29	0.093	0.134	0.92	5.11	5.93	1.62	3.69	7.17	1.75	6.17	0.125	0.280	4.12	3.35	2.97	1.66	0.91	1.09	4.24	0.035	0.098	
±	0.27	0.12	0.19	0.11	0.003	0.002	0.13	0.11	0.19	0.14	0.11	0.18	0.10	0.21	0.002	0.000	0.06	0.08	0.13	0.08	0.05	0.11	0.13	0.003	0.001	
NGC 3636	-1.82	0.48	-5.95	-1.61	0.064	0.101	1.01	5.04	5.39	1.57	3.91	6.12	1.91	5.09	0.108	0.249	3.82	3.23	2.78	1.55	0.85	0.91	3.31	0.040	0.099	
±	0.41	0.14	0.11	0.21	0.004	0.005	0.16	0.29	0.27	0.15	0.20	0.09	0.11	0.34	0.003	0.002	0.10	0.16	0.16	0.07	0.21	0.29	0.16	0.004	0.002	
NGC 3640	-1.82	0.01	-5.55	-0.97	0.128	0.178	1.19	5.39	5.93	1.48	3.37	7.16	2.06	6.00	0.143	0.289	3.97	3.29	2.88	1.76	1.09	1.14	3.49	0.046	0.082	
±	0.26	0.13	0.18	0.07	0.025	0.032	0.14	0.34	0.16	0.09	0.16	0.31	0.12	0.17	0.002	0.001	0.08	0.06	0.08	0.04	0.09	0.09	0.06	0.003	0.002	
NGC 3665	-1.18	1.14	-4.87	-0.46	0.085	0.128	1.28	4.64	6.12	1.62	3.56	8.07	2.18	5.13	0.152	0.309	4.14	3.19	2.91	1.86	1.08	1.03	4.13	0.035	0.099	
±	0.12	0.11	0.17	0.13	0.004	0.003	0.08	0.05	0.10	0.13	0.06	0.21	0.10	0.11	0.003	0.005	0.06	0.11	0.31	0.03	0.12	0.07	0.16	0.002	0.002	
NGC 3923 45°	-1.87	0.81	-6.86	-1.87	0.116	0.155	1.15	5.14	6.22	1.63	4.41	8.18	1.92	6.34	0.147	0.319	4.54	3.33	3.54	2.05	0.90	0.91	5.80	0.051	0.126	
±	0.24	0.09	0.15	0.04	0.010	0.005	0.16	0.25	0.29	0.15	0.20	0.03	0.08	0.33	0.005	0.005	0.08	0.10	0.08	0.07	0.03	0.09	0.06	0.003	0.002	
NGC 3923 90°	-3.63	-0.65	-5.54	-1.45	0.145	0.191	1.72	4.77	6.10	1.39	3.96	8.28	1.71	5.40	0.151	0.312	4.67	3.93	3.03	2.04	—	—	—	—	—	—
±	0.38	0.21	0.69	0.03	0.016	0.016	0.26	0.22	0.76	0.10	0.34	0.27	0.16	0.24	0.003	0.001	0.14	0.15	0.55	0.04	—	—	—	—	—	—
NGC 3941	-2.20	0.62	-6.49	-1.55	0.093	0.134	1.08	5.51	6.28	1.74	3.67	7.65	2.02	5.44	0.117	0.276	4.12	3.22	3.01	1.72	1.05	1.01	3.80	0.035	0.094	
±	0.08	0.05	0.17	0.11	0.001	0.002	0.06	0.09	0.18	0.04	0.13	0.24	0.07	0.14	0.005	0.002	0.05	0.05	0.07	0.06	0.03	0.04	0.10	0.002	0.001	
NGC 4125	-1.75	0.26	-5.82	-1.09	0.126	0.182	1.35	5.35	6.52	1.96	3.60	7.77	1.76	5.64	0.162	0.310	3.96	3.39	2.79	1.98	1.07	0.84	4.89	0.045	0.082	
±	0.18	0.12	0.13	0.09	0.002	0.003	0.07	0.08	0.16	0.15	0.08	0.06	0.10	0.45	0.002	0.003	0.10	0.11	0.12	0.13	0.01	0.08	0.11	0.004	0.001	
NGC 4261	-2.79	0.07	-6.57	-1.78	0.140	0.189	1.34	4.94	6.64	1.72	3.78	9.12	1.41	4.45	0.163	0.336	5.11	3.31	3.12	1.81	0.91	1.05	5.93	0.034	0.117	
±	0.16	0.26	0.34	0.14	0.004	0.005	0.13	0.32	0.19	0.08	0.06	0.21	0.12	0.33	0.003	0.002	0.08	0.10	0.10	0.16	0.17	0.21	0.19	0.005	0.005	
NGC 4365	-3.28	-0.06	-6.55	-1.56	0.172	0.225	1.30	5.15	6.38	1.74	3.69	8.11	1.73	5.57	0.175	0.345	4.73	3.48	3.13	2.24	0.92	0.90	5.56	0.055	0.098	
±	0.18	0.12	0.13	0.06	0.007	0.005	0.06	0.06	0.23	0.08	0.13	0.07	0.12	0.10	0.001	0.002	0.07	0.03	0.14	0.04	0.09	0.04	0.18	0.002	0.003	
NGC 4374	-2.43	0.31	-6.05	-1.34	0.123	0.168	1.42	5.06	5.91	1.44	3.87	7.41	1.84	5.06	0.148	0.306	4.68	2.90	3.12	1.86	0.81	0.87	4.52	0.037	0.104	
±	0.27	0.13	0.14	0.17	0.005	0.003	0.05	0.09	0.14	0.07	0.14	0.11	0.11	0.23	0.001	0.001	0.06	0.12	0.18	0.09	0.07	0.06	0.09	0.002	0.003	
NGC 4494 0°	-1.02	0.65	-5.99	-1.49	0.103	0.157	1.13	5.31	5.41	1.63	4.28	7.98	1.77	6.11	0.137	0.275	3.90	3.09	2.68	1.68	0.94	0.89	3.93	0.042	0.080	
±	0.10	0.08	0.17	0.01	0.002	0.002	0.02	0.17	0.11	0.03	0.07	0.19	0.01	0.04	0.002	0.002	0.08	0.05	0.06	0.04	0.03	0.02	0.04	0.003	0.001	
NGC 4494 90°	—	—	—	—	—	—	—	—	—	—	—	—	—	—	—	—	—	—	—	—	—	—	—	—	—	
±	—	—	—	—	—	—	—	—	—	—	—	—	—	—	—	—	—	—	—	—	—	—	—	—	—	
NGC 4550	-0.02	1.93	-3.78	-0.40	-0.027	0.008	1.23	3.85	4.69	1.36	-0.05	4.64	2.24	4.03	0.079	0.213	3.44	2.83	2.80	1.43	1.02	0.69	2.88	0.026	0.075	
±	0.11	0.21	0.38	0.20	0.004	0.005	0.27	0.17	0.36	0.02	2.87	0.43	0.37	0.12	0.001	0.002	0.04	0.35	0.33	0.15	0.22	0.11	0.08	0.002	0.003	
NGC 4754	-3.23	0.12	-6.92	-1.87	0.135	0.181	1.42	5.35	6.60	1.81	3.90	9.01	1.59	6.40	0.178	0.357	4.60	3.73	3.40	1.86	0.86	0.87	4.52	0.042	0.103	
±	0.14	0.04	0.13	0.09	0.003	0.004	0.05	0.05	0.14	0.08	0.08	0.13	0.09	0.15	0.003	0.004	0.06	0.12	0.08	0.06	0.04	0.10	0.14	0.002	0.001	
NGC 5322	-0.96	0.76	-6.15	-1.44	0.103	0.161	1.37	5.36	6.04	1.80	3.72	8.27	2.08	6.03	0.149	0.301	4.16	3.42	2.90	1.98	1.03	1.18	4.36	0.043	0.083	
±	0.14	0.14	0.05	0.02	0.005	0.004	0.06	0.06	0.07	0.09	0.14	0.11	0.09	0.14	0.001	0.002	0.08	0.05	0.11	0.07	0.01	0.07	0.04	0.001	0.004	
NGC 5353	-1.23	0.50	-7.08	-1.93	0.159	0.212	1.31	5.15	6.48	1.93	3.96	10.31	1.68	6.24	0.201	0.371	5.18	3.73	3.55	1.81	0.81	1.13	6.74	0.058	0.101	
±	0.45	0.24	0.16	0.14	0.014	0.020	0.10	0.24	0.21	0.07	0.08	0.43	0.09	0.19	0.003	0.001	0.10	0.16	0.15	0.10	0.10	0.15	0.10	0.000	0.004	
NGC 5354 90°	-2.09	0.23	-6.30	-1.63	0.087	0.124	1.20	5.27	5.75	1.59	4.08	6.75	1.17	4.22	0.135	0.296	4.01	3.39	2.92	1.54	0.65	1.05	4.29	0.024	0.094	
±	0.25	0.33	0.18	0.18	0.013	0.013	0.20	0.30	0.05	0.14	0.23	0.17	0.51	0.005	0.009	0.21	0.06	0.11	0.07	0.12	0.08	0.08	0.13	0.005	0.004	
NGC 5354 0°	-1.65	0.39	-6.92	-1.91	0.095	0.146	1.18	5.36	5.95	1.36	3.71	8.04	1.56	5.17	0.166	0.320	4.59	3.19	3.01	2.17	0.94	0.88	4.81	0.045	0.090	
±	0.35	0.33	0.12	0.09	0.005	0.004	0.06	0.09	0.32	0.17	0.22	0.28	0.12	0.17	0.005	0.004	0.13	0.19	0.20	0.11	0.11	0.03	0.14	0.003	0.001	
NGC 5363	-2.02	-0.06	-5.31	-1.09	0.152	0.200	0.79	5.01	5.61	1.41	3.03	6.34	1.98	4.15	0.160	0.293	4.01	3.00	2.24	1.68	1.05	1.12	6.47	0.044	0.100	
±	0.42	0.24	0.25	0.15	0.018	0.016	0.23	0.12	0.18	0.08	0.10	0.40	0.19	0.20	0.005	0.007	0.19	0.11	0.15	0.07	0.05	0.04	0.11	0.002	0.001	
NGC 5444	-2.68	0.23	-6.60	-1.80	0.124	0.170	1.41	5.61	6.07	1.43	4.15	8.21	1.19	5.79	0.141	0.329	4.88	3.01	3.30	1.94	0.78	0.83	5.24	0.021	0.097	
±	0.12	0.11	0.43	0.14	0.009	0.010	0.17	0.34	0.24	0.12	0.25	0.44	0.09	0.16	0.002	0.005	0.07	0.13	0.05	0.06	0.10	0.14	0.22	0.005	0.001	
NGC 5557	-2.04	0.14	-5.93	-1.42	0.098	0.130	1.27	5.16	5.98	1.55	3.55	7.89	1.62	5.95	0.137	0.308	4.55	3.38	3.06	1.86	0.90	1.05	5.10	0.034		

Table B1. Fully corrected Lick/IDS indices for the central $r_e/8$ extraction: continued.

Galaxy	$H\delta_A$ [Å]	$H\delta_F$ [Å]	$H\gamma_A$ [Å]	$H\gamma_F$ [Å]	CN_1 [mag]	CN_2 [mag]	Ca4227 [Å]	G4300 [Å]	Fe4383 [Å]	Ca4455 [Å]	Fe4531 [Å]	C ₂ 4668 [Å]	$H\beta$ [Å]	Fe5015 [Å]	Mg ₁ [mag]	Mg ₂ [mag]	Mg _b [Å]	Fe5270 [Å]	Fe5335 [Å]	Fe5406 [Å]	Fe5709 [Å]	Fe5782 [Å]	NaD [Å]	TiO ₁ [mag]	TiO ₂ [mag]			
NGC 5812	-2.34	-0.04	-6.97	-2.14	0.141	0.191	1.27	5.27	6.08	1.54	3.98	8.74	1.63	6.51	0.153	0.336	4.92	3.49	3.38	1.95	0.80	0.90	5.62	0.034	0.102			
±	0.11	0.10	0.44	0.49	0.005	0.004	0.07	0.21	0.32	0.11	0.12	0.22	0.06	0.10	0.003	0.002	0.13	0.05	0.05	0.07	0.07	0.03	0.09	0.003	0.003			
NGC 5813	-3.50	-0.07	-6.80	-2.17	0.085	0.119	1.59	5.70	5.81	1.81	4.05	8.07	1.58	4.69	—	—	4.64	3.01	2.67	1.85	0.81	1.09	4.63	0.047	0.096			
±	0.13	0.09	0.15	0.09	0.003	0.003	0.09	0.17	0.24	0.10	0.15	0.30	0.11	0.22	—	—	0.06	0.05	0.11	0.09	0.04	0.08	0.06	0.003	0.001			
NGC 5831	-2.48	0.55	-5.63	-1.28	0.117	0.160	1.19	4.75	6.19	1.52	3.87	7.97	1.47	5.94	0.158	0.328	4.58	3.42	3.27	1.69	0.96	0.97	4.44	0.036	0.105			
±	0.15	0.09	0.29	0.13	0.008	0.008	0.19	0.17	0.26	0.11	0.14	0.42	0.14	0.24	0.007	0.007	0.05	0.14	0.08	0.11	0.07	0.10	0.06	0.004	0.004			
NGC 5845	-2.65	0.05	-6.05	-1.57	0.140	0.197	1.48	5.59	5.60	1.77	3.99	7.48	1.93	5.65	0.175	0.330	4.56	3.37	3.23	1.88	1.03	0.89	4.79	0.045	0.083			
±	0.37	0.13	0.08	0.04	0.005	0.006	0.07	0.14	0.21	0.13	0.15	0.28	0.09	0.16	0.003	0.004	0.13	0.08	0.09	0.07	0.12	0.08	0.09	0.002	0.004			
NGC 5846 0°	-2.50	0.27	-7.03	-1.87	0.120	0.157	0.68	5.92	6.75	1.48	3.70	9.07	1.52	4.48	0.171	0.331	4.74	3.17	2.92	1.88	0.94	1.00	5.12	0.051	0.090			
±	0.30	0.21	0.24	0.12	0.023	0.026	0.23	0.16	0.20	0.10	0.12	0.37	0.11	0.12	0.002	0.007	0.05	0.11	0.17	0.04	0.03	0.04	0.08	0.002	0.003			
NGC 5846 90°	—	—	—	—	—	—	—	—	—	—	—	—	—	—	—	—	—	—	—	1.83	0.77	0.86	5.00	0.045	0.113			
±	—	—	—	—	—	—	—	—	—	—	—	—	—	—	—	—	—	—	—	0.14	0.07	0.07	0.14	0.002	0.001			
NGC 5846 A	-2.43	0.44	-5.91	-1.59	0.120	0.167	0.89	5.52	4.79	1.58	4.21	7.17	1.48	5.84	0.152	0.312	4.51	2.96	3.01	1.63	0.74	0.82	4.67	0.048	0.095			
±	0.25	0.37	0.13	0.17	0.024	0.029	0.24	0.20	0.26	0.21	0.34	0.45	0.17	0.33	0.008	0.004	0.24	0.17	0.33	0.11	0.09	0.02	0.07	0.001	0.004			
NGC 5854	—	—	—	—	—	—	—	—	—	—	—	—	—	—	—	—	—	—	—	2.50	2.20	1.23	1.02	0.73	0.39	2.69	0.033	0.083
±	—	—	—	—	—	—	—	—	—	—	—	—	—	—	—	—	—	—	—	0.17	0.14	0.09	0.11	0.10	0.06	0.003	0.003	
NGC 5864	-1.72	0.58	-5.03	-0.62	0.014	0.053	1.22	5.07	5.52	1.14	3.47	6.15	2.02	6.20	0.093	0.211	2.78	2.79	2.71	1.50	1.07	0.37	3.14	0.027	0.094			
±	0.18	0.23	0.14	0.16	0.007	0.005	0.13	0.22	0.29	0.08	0.25	0.20	0.09	0.42	0.002	0.002	0.15	0.15	0.13	0.08	0.11	0.11	0.05	0.004	0.004			
NGC 5869	—	—	—	—	—	—	—	—	—	—	—	—	—	—	—	—	—	—	—	1.88	0.80	1.02	4.25	0.033	0.107			
±	—	—	—	—	—	—	—	—	—	—	—	—	—	—	—	—	—	—	—	0.08	0.08	0.05	0.20	0.003	0.001			
NGC 5982	-2.04	0.27	-5.86	-1.37	0.099	0.142	1.40	5.24	5.86	1.78	3.75	8.99	1.47	5.88	0.129	0.300	4.44	3.16	3.04	1.76	0.66	1.14	4.96	0.034	0.102			
±	0.17	0.14	0.15	0.03	0.006	0.008	0.03	0.12	0.20	0.21	0.11	0.18	0.07	0.26	0.002	0.003	0.11	0.14	0.09	0.09	0.04	0.08	0.06	0.002	0.002			
NGC 6172	1.04	1.98	-3.31	-0.26	0.010	0.048	0.61	4.20	4.56	1.22	3.09	7.59	2.48	4.72	0.080	0.210	2.94	2.88	2.52	1.20	0.89	1.23	4.00	0.036	0.076			
±	0.17	0.15	0.20	0.21	0.005	0.005	0.06	0.12	0.31	0.11	0.09	0.25	0.15	0.37	0.009	0.008	0.11	0.11	0.10	0.07	0.04	0.05	0.07	0.003	0.005			
NGC 6411	-1.40	0.58	-6.18	-1.47	0.040	0.073	1.15	5.45	6.20	1.54	3.84	6.95	1.71	5.41	0.123	0.284	3.84	3.33	2.36	1.46	0.94	0.82	3.88	0.035	0.116			
±	0.27	0.17	0.13	0.09	0.010	0.006	0.05	0.17	0.41	0.14	0.15	0.22	0.01	0.38	0.002	0.004	0.05	0.10	0.17	0.05	0.05	0.05	0.10	0.002	0.002			
NGC 7302	-1.67	0.64	-5.62	-1.31	0.060	0.098	1.25	4.73	6.46	1.44	4.51	7.66	1.94	6.48	0.105	0.259	3.62	3.45	2.75	1.84	0.93	0.97	3.71	0.038	0.086			
±	0.61	0.14	0.28	0.20	0.025	0.033	0.11	0.37	0.13	0.21	0.52	0.20	0.10	0.20	0.002	0.003	0.18	0.10	0.16	0.09	0.06	0.07	0.09	0.002	0.006			
NGC 7332	-1.26	1.03	-5.09	-0.49	0.047	0.085	1.09	5.20	6.02	1.52	4.16	7.67	2.49	6.82	0.117	0.248	3.79	3.30	2.90	1.71	1.05	0.97	4.18	0.042	0.078			
±	0.13	0.11	0.07	0.04	0.008	0.009	0.06	0.19	0.27	0.03	0.34	1.12	0.26	0.10	0.008	0.011	0.10	0.06	0.05	0.05	0.04	0.03	0.03	0.004	0.003			
NGC 7454	-0.50	1.22	-4.66	-0.55	0.024	0.069	1.26	5.39	4.79	1.57	3.58	6.60	2.21	5.78	0.095	0.223	3.29	2.76	2.32	1.54	0.91	0.55	2.45	0.033	0.059			
±	0.51	0.33	0.13	0.08	0.011	0.013	0.13	0.16	0.22	0.12	0.22	0.50	0.13	0.28	0.005	0.002	0.04	0.08	0.09	0.08	0.08	0.08	0.09	0.001	0.003			
NGC 7585	1.36	2.02	-2.82	0.36	-0.018	0.032	1.10	3.90	5.57	1.66	3.57	6.84	2.65	5.27	0.108	0.256	3.45	3.08	2.58	1.66	0.83	1.11	4.29	0.032	0.068			
±	0.13	0.13	0.16	0.08	0.006	0.007	0.05	0.06	0.11	0.07	0.09	0.47	0.17	0.15	0.002	0.002	0.05	0.12	0.31	0.04	0.04	0.04	0.08	0.001	0.000			
NGC 7619	-3.40	-0.18	-6.89	-1.98	0.136	0.194	2.06	5.55	6.59	2.24	4.21	10.04	1.48	6.22	0.156	0.328	5.32	3.75	3.83	2.32	1.13	1.21	5.85	0.056	0.104			
±	0.09	0.08	0.11	0.06	0.006	0.007	0.13	0.10	0.12	0.17	0.13	0.19	0.09	0.19	0.002	0.001	0.07	0.06	0.11	0.06	0.05	0.05	0.04	0.003	0.005			
NGC 7626	-3.29	-0.16	-6.47	-1.83	0.131	0.187	1.48	4.95	5.54	1.89	3.41	8.77	1.33	5.83	0.156	0.335	5.07	3.20	3.42	1.92	0.94	1.19	5.74	0.048	0.107			
±	0.23	0.24	0.23	0.12	0.008	0.009	0.13	0.25	0.32	0.24	0.28	0.34	0.12	0.18	0.003	0.002	0.12	0.09	0.17	0.11	0.03	0.05	0.03	0.003	0.005			